THESIS

CROSS BEAM WIND MEASURING TECHNIQUES

Submitted by

Benjamin Cory Hablutzel

In partial fulfillment of the requirements

for the Degree of Master of Science

Colorado State University

Fort Collins, Colorado

ABSTRACT OF THESIS

CROSS BEAM WIND MEASURING TECHNIQUES

The usefulness of the cross beam technique for measuring atmospheric wind speeds is discussed. Two remote photodetectors monitor the light scattering mainly from dust, water vapor, and atmospheric pollutants, which serve as tracers for the mean wind speed. The time required for the particles to travel from one beam to another (transit time) is computed by space-time correlations of the two signals. The transit time occurs at the maximum correlation between the fluctuations in the two signals. Since the beam separation is known, the wind speed may be computed, once the transit time is known.

Six experimental wind measurements using varying beam separations are discussed. To provide a basis for comparison, the wind speeds were monitored by cup anemometers. Four of the six experiments yielded wind speeds comparable to the dominant speeds obtained from the anemometers. It had been assumed that the common signals yielded positive correlations, but it was suggested that the aerosols might scatter light into one beam and away from the other, making the correlations negative. If there is an equal likelihood of positive and negative correlations by the common signal, the resulting correlation does not have a maximum value at the desired transit time. This may have been the case for the two remaining experiments. The possibility also existed that the beam separations of the two remaining experiments may have been too long, so that there were no signals common to both beams.

It is concluded that the cross beam technique for measuring atmospheric winds works some of the time. Although the present setup cannot be used on an operational basis, the concepts may prove successful

using artificial light sources or wavelengths other than those in the visual range.

Benjamin Cory Hablutzel
Atmospheric Science Department
Colorado State University
Fort Collins, Colorado 80521
June, 1970

ACKNOWLEDGEMENTS

The author wishes to express his appreciation to Professors Virgil A. Sandborn and Elmar R. Reiter for their guidance during this research. Appreciation is also expressed to Dr. Peter C. Sinclair for taking time to read and comment on the manuscript. A sincere thanks is expressed to Dr. F. R. Krause, NASA Marshall Space Flight Center (MSFC), Mr. J. B. Stephens, MSFC, Mr. R. R. Jayroe, Jr., MSFC, and Dr. M.-Y. Su, Northrop, for their guidance and major assistance in the overall program. The tests were conducted by Mr. Earl Klugman, Illinois Institute of Technology Research Institute (IITRI), and Mr. David Pickelner, CSU. Data processing and interpretation were performed by Mr. Jack Jones, MSFC, Mr. William C. Cliff, MSFC, Mr. John Pooley, Northrop, and Mr. Mel Phillips, IITRI. Dr. A. J. Montgomery, IITRI, designed and checked out the detection system. This research was performed under the National Aeronautics and Space Administration (NASA) Contract No. NAS8-21049, Control No. DCN 1-7-75-20042(IF).

TABLE OF CONTENTS

LIST OF TABLES

LIST OF FIGURES

LIST OF FIGURES (Continued)

LIST OF SYMBOLS

e^2 = energy estimate at a given frequency

e_T^2 = estimate of total energy

f = frequency

f_{MAX} = maximum frequency

h = time lag width

i = piece number

m = number of pieces

$R_X(\tau)$ = autocorrelation of X at a time delay τ

$R_Y(\tau)$ = autocorrelation of Y at a time delay τ

$R_{XY}(\tau)$ = cross correlation of X and Y at a time delay τ

$\hat{R}_{XY}(\tau) = \dfrac{R_{xy}(\tau)}{[R_x(o)]^{1/2}[R_y(o)]^{1/2}}$

$S(f)$ = power spectral density at frequency f

$\hat{S}(f) = S(f)/e_T^2$

t = time

$t' = t - \tau$

T = record length

ΔT = piece length

v = wind speed

$x(t)$ = deviation from $\overline{X(t)}$

x_+ = x if $x \geq 0$ and zero if $x \leq 0$

x_- = zero if $x \geq 0$ and x if $x \leq 0$

$X(t)$ = light intensity from Beam A at time t

$\overline{X(t)}$ = mean of $X(t)$

$y(t)$ = deviation from $\overline{Y(t)}$

y_+ = y if $y \geq 0$ and zero if $y \leq 0$

y_- = zero if $y \geq 0$ and y if $y \leq 0$

$Y(t)$ = light intensity from Beam B at time t

$\overline{Y(t)}$ = mean of $Y(t)$

μ_X = mean of X

μ_Y = mean of Y

ξ = beam separation

τ = time delay

τ_m = time delay corresponding to the maximum correlation

τ_{max} = maximum time delay

$\Delta\tau$ = time delay width

$\overline{(\ )}_i$ = time average over the ith piece

$\overline{(\ )}_m$ = time average over m pieces

INTRODUCTION

A remote sensing technique for measuring wind speeds, called the cross beam method, has been developed. The validity of the method has been established in the wind tunnel (Fisher and Krause, 1967) and the technique has been adapted to provide experimental results in the atmosphere (Stephens and Sandborn, 1968).

The wind speeds may be detected by monitoring the space and time variations of skylight emission with two remote photodetectors and then correlating the two signals. The correlations may be determined by analog or digital methods.

The objective is to examine wind speed computations obtained from the analog and digital methods and to examine differences in the computed wind speeds, as well as to determine how the results compare with those obtained from cup anemometers.

Fisher and Krause (1965) and Wolff (1966) proposed cross beam test arrangements. Fisher compared cross beam results with hot wire results in a subsonic round jet to try to establish the true resolution of turbulence parameters in jet shear layers. The velocities, eddy lifetimes, and moving axis autocorrelation curves obtained by the cross beam method agreed with hot wire measurements within the experimental error of the hot wire (Fisher and Krause, 1967). Wolff tried to determine the height of the maximum airglow intensity. Two telescopes scanned the upper atmosphere so that the intersection of their fields moved repeatedly along horizontal lines. The altitude of the maximum airglow emission was then assumed to be the "crossing height" at which the maximum beam covariance occurred. This experiment was also successful.

Atmospheric cross beam tests were first conducted at the George C. Marshall Space Flight Center near Huntsville, Alabama during the summer of 1967. Later tests were conducted at the Colorado State University Meteorological Tower near Platteville, Colorado, and the Environmental Science Services Administration (ESSA) test sites at Gun Barrel Hill near Boulder, Colorado, and near Haswell, Colorado.

THE CROSS BEAM TECHNIQUE

By using optical beams, information may be obtained from a flow field by monitoring the light fluctuations, which are related to light scattering mainly from dust, water vapor, and atmospheric pollutants (Fisher and Krause, 1967; Sandborn and Pickelner, 1969). Since the particles are carried by the mean wind speed, they serve as tracers for the mean wind speed, which is determined by measuring the time required for the tracers to travel a given path.

The cross beam system uses two narrow view telescopes and may be used with any wavelength. The field experiments were made for optical wavelengths between .45 and .65 microns. The telescopes view different backgrounds and optical paths. The light fluctuations seen by both telescopes are from the same aerosol scattering and may be retrieved by space-time correlations. Figure 1 shows a schematic diagram of the cross beam system. The ground based telescopes are pointed skyward and are oriented so that the beams are normal to the mean wind direction and the minimum beam separation is at tower height; therefore, only the tracers at tower height will pass through both beams. At other altitudes, only one of the two beams will monitor the light fluctuations.

To obtain the common signal from the two telescopes, a time-delayed correlation between the two signals is measured. This is done by delaying the output from the upstream beam and correlating it with the output from the downstream beam. The maximum correlation is obtained when the time delay is equal to the time required for the aerosols to travel from the upstream beam to the downstream beam. Since the aerosols are carried by the turbulent flow, an individual particle does not travel in a straight

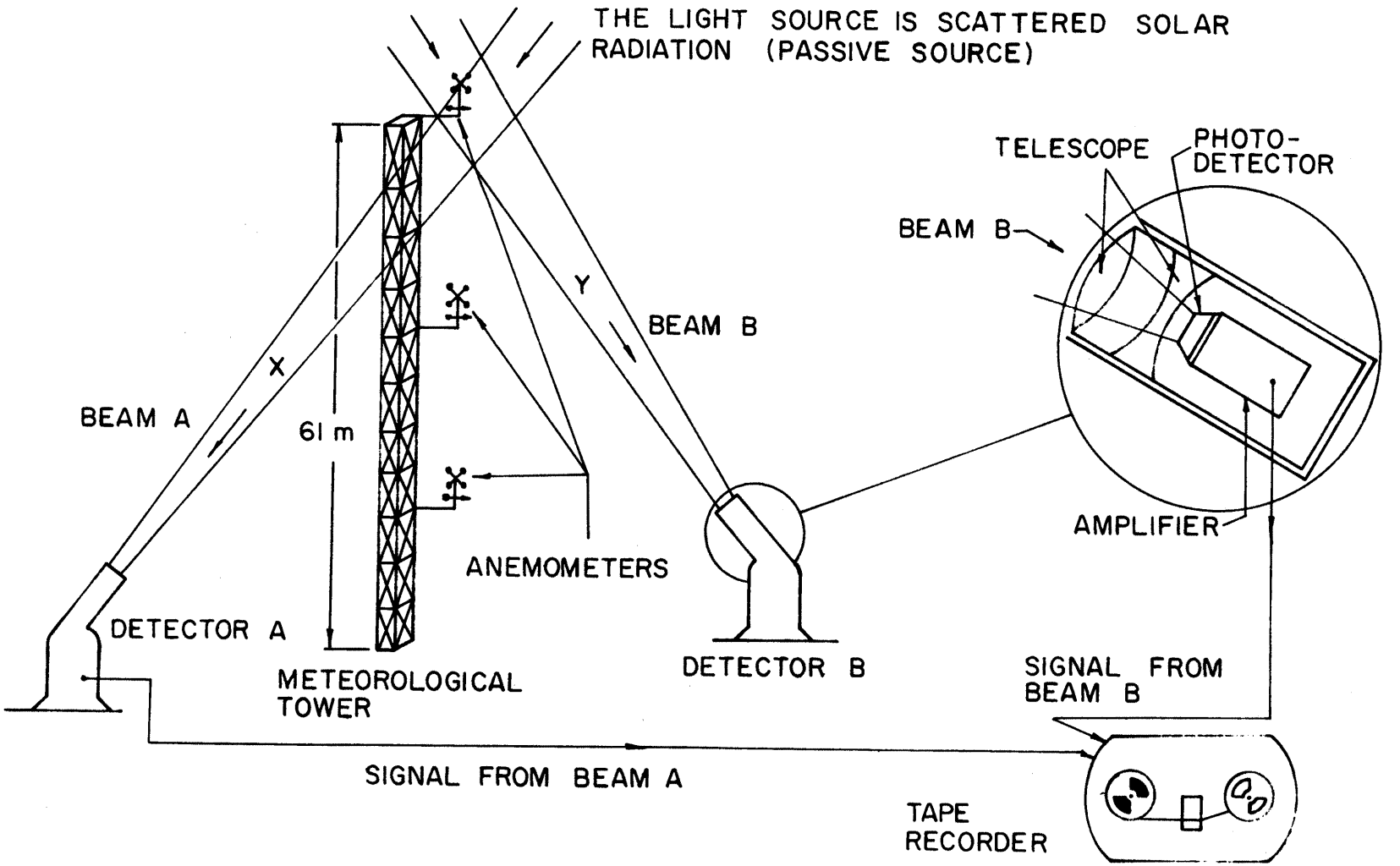

Figure 1. Cross beam detection system.

path and its velocity may exceed or be slower than the mean wind speed by an amount equal to the turbulent speed component. The integration time must be sufficiently long enough to average out the turbulent fluctuations and to obtain a sufficient sample of events related to both beams.

Figures 2 and 3 show the field station electronics and one of two telescope units. The telescopes' field of view is spread approximately 30 minutes and a silicon diode collects the light fluctuations. D.C. drift and 1/f noise from the photodiode were eliminated by a chopper, which operated approximately 1000 cycles per second in front of the photodiode. The photodiode output was amplified and filtered for frequencies between .01 and 10 cycles per second. Wind velocities from cup anemometers were recorded simultaneously.

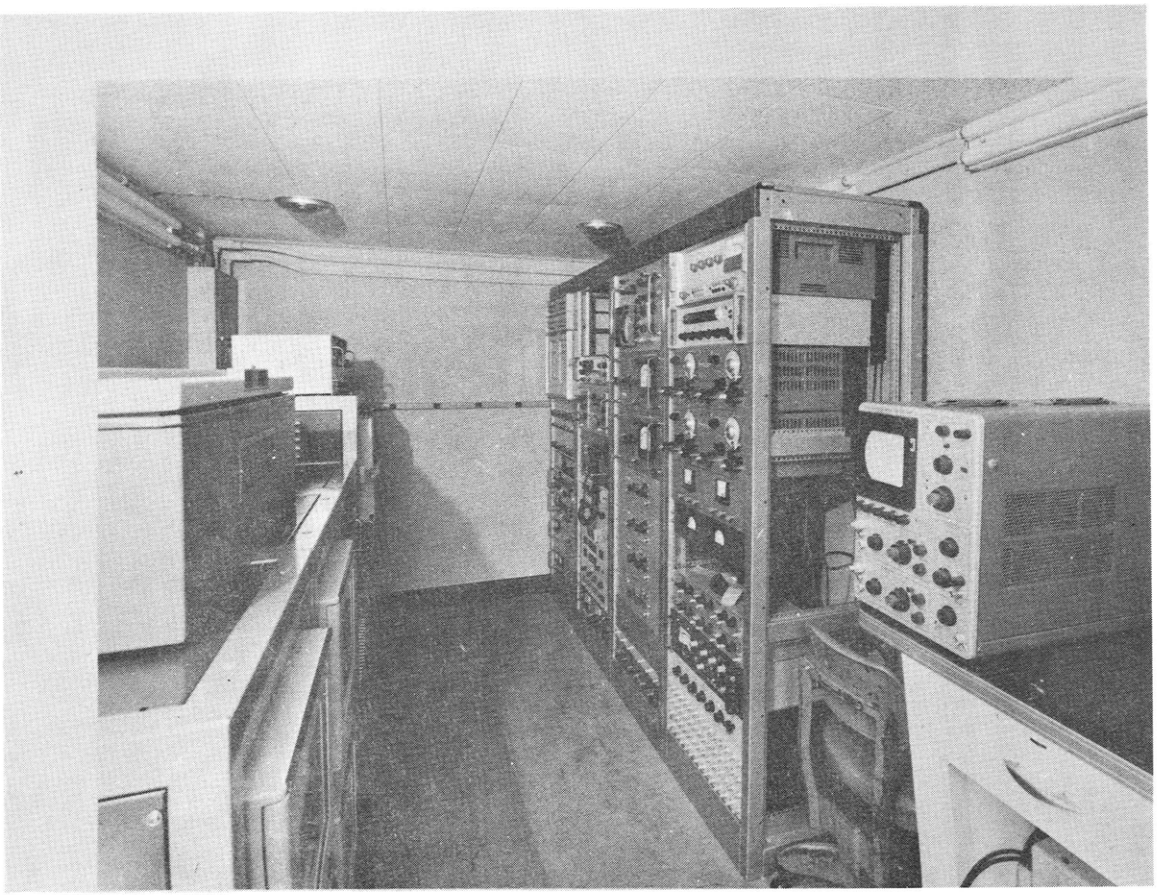

Figure 2. Inside of instrumentation and analog computation van.

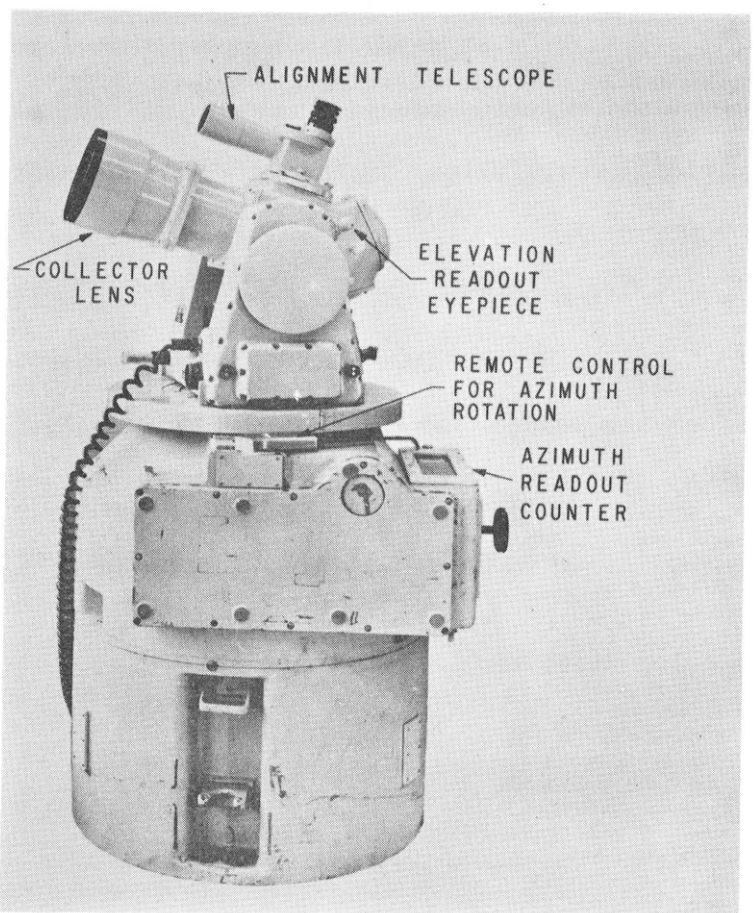

Figure 3. Optical cross beam photometer unit.

ANALOG DATA REDUCTION

The Princeton Applied Research (PAR) Model 101 Correlation Function Computer (Figure 4) was used (Szmauz, 1967). One hundred points of the correlation function are computed and stored for readout. The total delay time ranges from 100 milliseconds to 10 seconds plus a provision for starting the computation at delay times other than zero. For example, if the basic computation period ranges from $0 \leq \tau \leq 10$, it is possible to compute additional correlations in the delay time ranges $20 \leq \tau \leq 30$, ..., $90 \leq \tau \leq 100$.

Sampling errors from the correlation computations must be considered (Klugman, 1969). To define the data at a given frequency, at least two correlation values are needed. The lag width $\Delta\tau$ (Bendat and Piersol, 1966) is given by

$$\Delta\tau \leq \frac{1}{2f_{MAX}} \quad . \tag{1}$$

One may assign a lag width as

$$\Delta\tau = \frac{1}{4f_{MAX}} \quad , \tag{2}$$

$$f \leq \frac{1}{4\Delta\tau} \quad . \tag{3}$$

The maximum time lag is divided into 100 equal time lag intervals. Since correlations for negative as well as positive lags are being considered, the total number of time lag intervals is 200. Therefore

$$\frac{1}{200\Delta\tau} \leq f \leq \frac{1}{4\Delta\tau} \quad , \tag{4}$$

$$\frac{1}{4\Delta\tau} = \frac{50}{200\Delta\tau} = \frac{50}{2\tau_{MAX}} \quad , \tag{5}$$

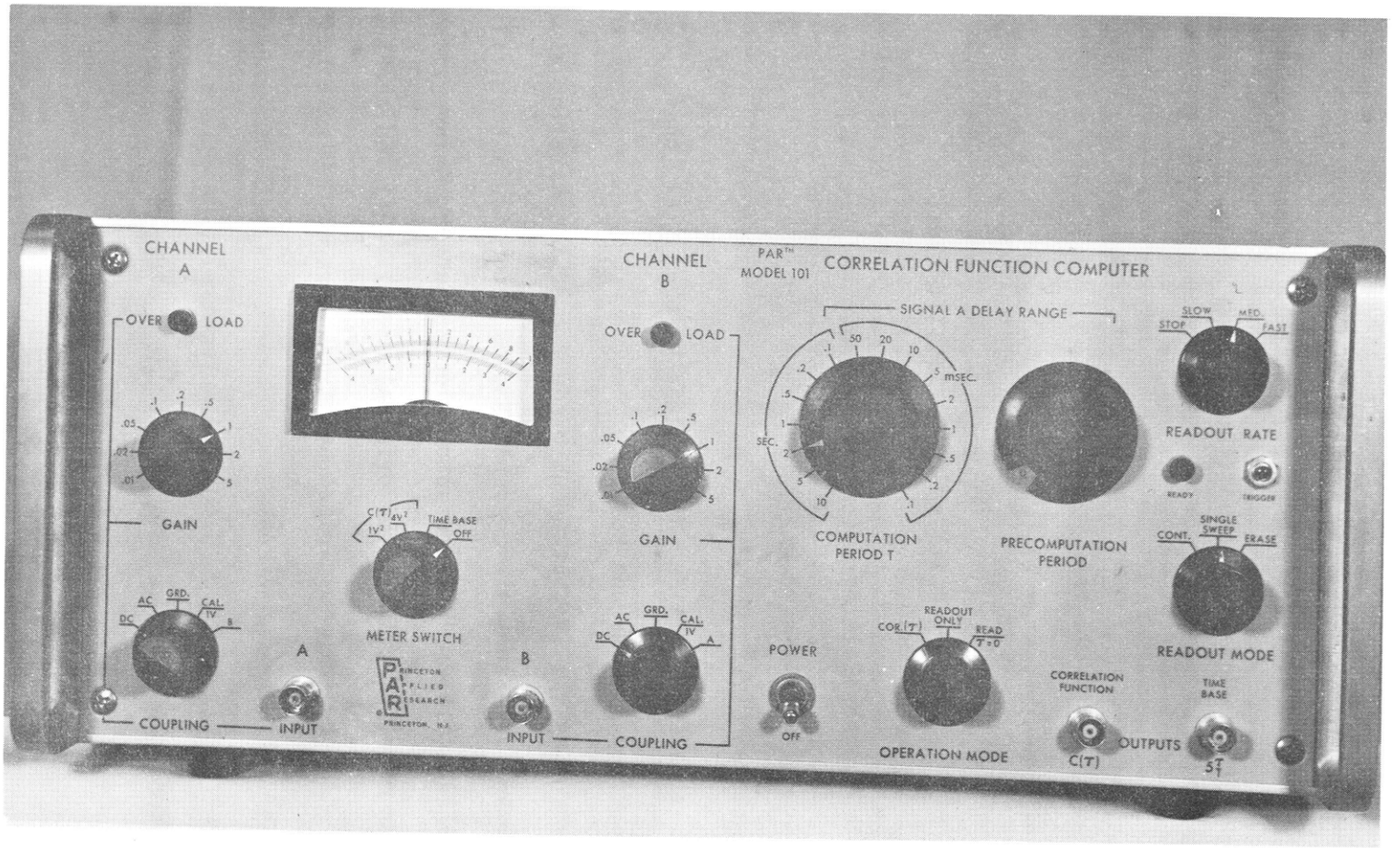

Figure 4. PAR Model 101 signal correlator.

$$\frac{1}{2\tau_{MAX}} \leq f \leq \frac{25}{\tau_{MAX}} \quad , \tag{6}$$

where τ_{MAX} is the maximum time delay. The filters (Figure 5) are then set to include the frequency range described above. The experiments were recorded at a speed of 1 7/8 inches per second and each experiment was correlated at 60 inches per second (the maximum speed on the recorder) or a speedup by a factor of 32.

Autocorrelation Measurements

The autocorrelation of a signal X from beam A is given by

$$R_X(\tau) = \frac{1}{T} \int_0^T X(t)X(t+\tau)dt, \tag{7}$$

where T is the total integration time (Bendat and Piersol, 1966). The autocorrelation is estimated by:

1. Delaying X(t) by a lag time τ.
2. Multiplying X(t) at any instant by the x(t) that occurred τ seconds before.
3. Averaging the instantaneous product over the sampling time.

The above operations are accomplished by an analog autocorrelation function (ACF) analyzer, which uses an electronic time delay circuit to displace the signal in time. The original signal X(t) and the delayed signal $X(t-\tau)$ are then multiplied and time averaged. Figure 6 shows a block diagram for an ACF analyzer.

The same requirements hold for the autocorrelation of a signal from beam B, given by

$$R_Y(\tau) = \frac{1}{T} \int_0^T Y(t)Y(t+\tau)dt \ . \tag{8}$$

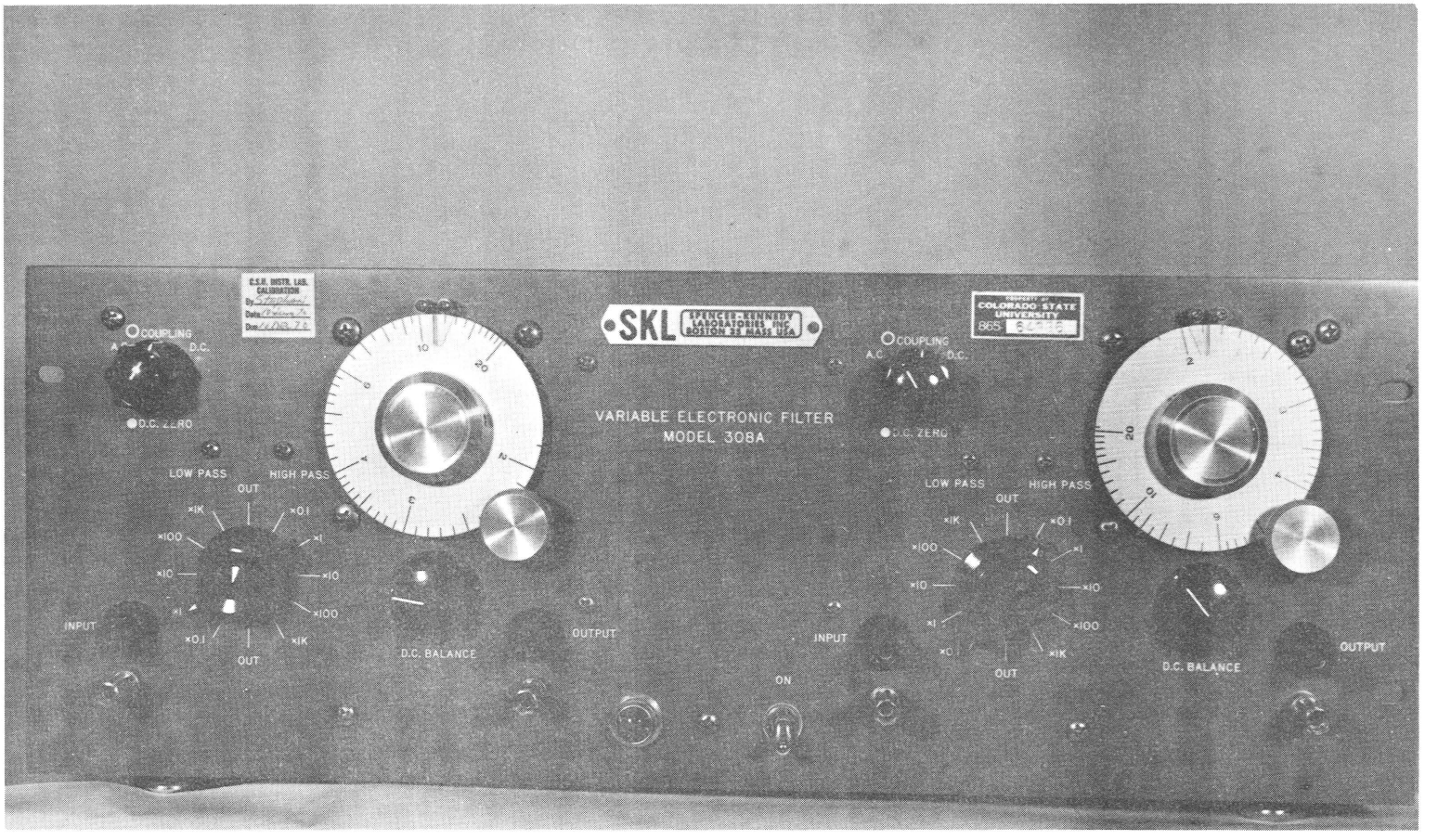

Figure 5. Variable electronic filter.

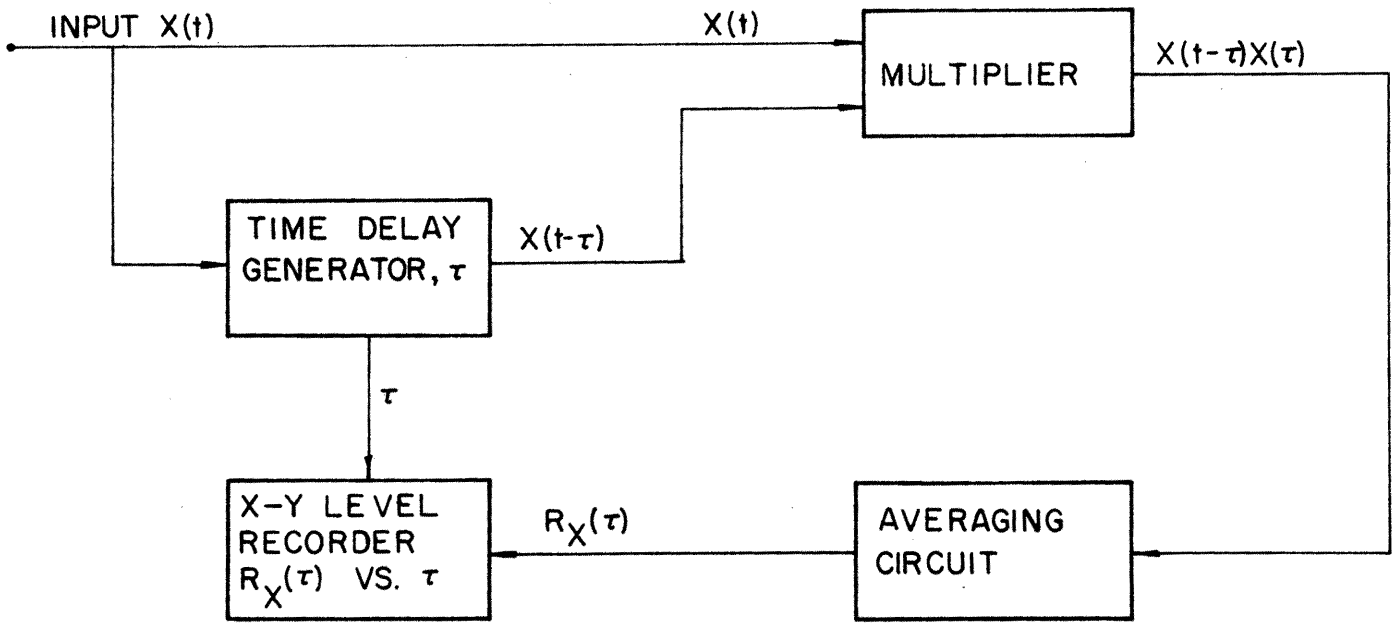

Figure 6. Functional block diagram for autocorrelation analyzer. (Bendat and Piersol, 1966)

Cross Correlation Measurements

The cross correlation of signals X and Y from beams A and B respectively is given by

$$R_{XY}(\tau) = \frac{1}{T} \int_0^T X(t)Y(t+\tau)dt \ , \qquad (9)$$

and is estimated by:

1. Delaying X(t) relative to Y(t) by a lag time τ.
2. Multiplying Y(t) at any instant by the X(t) that occurred τ seconds before.
3. Averaging the instantaneous product over the sampling time.

The above operations are accomplished by a cross correlation function (CCF) analyzer, which is exactly the same as an ACF analyzer, except that the direct imput to the multiplier and the input to the lag time generator are independent. Figure 7 shows a block diagram for a CCF analyzer. Computations using negative time delays are accomplished in the same manner as above, except that Y(t) is delayed relative to X(t).

Applications

Since different sets of correlations are to be examined and compared, certain standards are necessary. The means of X(t) and Y(t) (μ_X and μ_Y) should be zero over the integration time. If, for example, μ_X were not zero, the autocorrelation would approach μ_X^2 for large t. By shifting the ordinate so that μ_X^2 is zero, the nonzero means are effectively eliminated (Bendat and Piersol, 1966). For the correlations being considered, the means were close enough to zero that shifts were not necessary. The cross correlations are then normalized, or

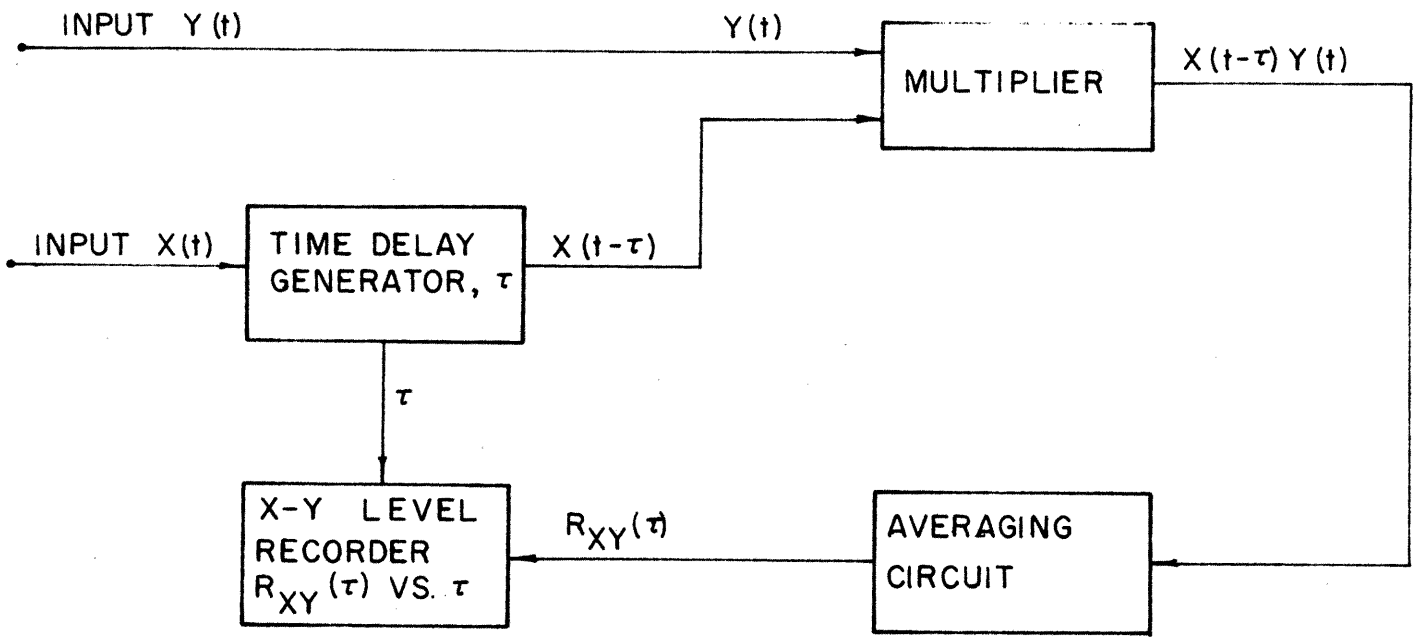

Figure 7. Functional block diagram for cross correlation analyzer. (Bendat and Piersol, 1966)

$$R_{XY}(\tau) = \frac{R_{XY}(\tau)}{[R_X(o)]^{1/2}[R_Y(o)]^{1/2}} \tag{10}$$

As mentioned previously, the maximum correlation is obtained when the time delay is equal to the time required for the aerosols to travel from the upstream beam to the downstream beam. Since the beam separation is already known, the wind speed is given by

$$v = \xi/\tau_m \ , \tag{11}$$

where ξ is the beam separation and τ_m is the time delay corresponding to the maximum correlation. If the beam separation is zero, no wind speed can be determined and the maximum correlation will occur at zero time lag.

DIGITAL DATA REDUCTION

Digitizing consists of converting continuous data into discrete numbers (Bendat and Piersol, 1966). The process is achieved by sampling, which defines the points at which the data are observed. Enough samples must be made to obtain the significant information. If the sample points are too close together, the amount of labor and calculations will increase. The sampling rate should be the lowest possible. If the time interval between samples is h seconds (Figure 8), the useful data will be from zero to the cutoff frequency of $1/2h$ cycles per second (cps), known as the Nyquist frequency. If the original data consists of frequencies predominately higher than $1/2h$ cps, the sampling rate will yield information with erroneous frequencies, a property known as aliasing. An upper limit of $1/4h$ cps is used here.

The Piecewise Operation

The purpose of this operation is to overcome computer storage limitations (Krause, Jones, and Fisher, 1967). A record of length T is broken into m pieces of length ΔT so that $T = m\Delta T$. Data may be stored at any one time only from an individual piece. Figure 9 shows a subdivision of a record.

The time average of the data over the ith piece is given by

$$\overline{(\ )}_i = \frac{1}{\Delta T} \int_{t=(i-1)\Delta T}^{t=i\Delta T} (\ )dt \ . \qquad (12)$$

The mean of the entire record is the arithmetic mean over all pieces, given by

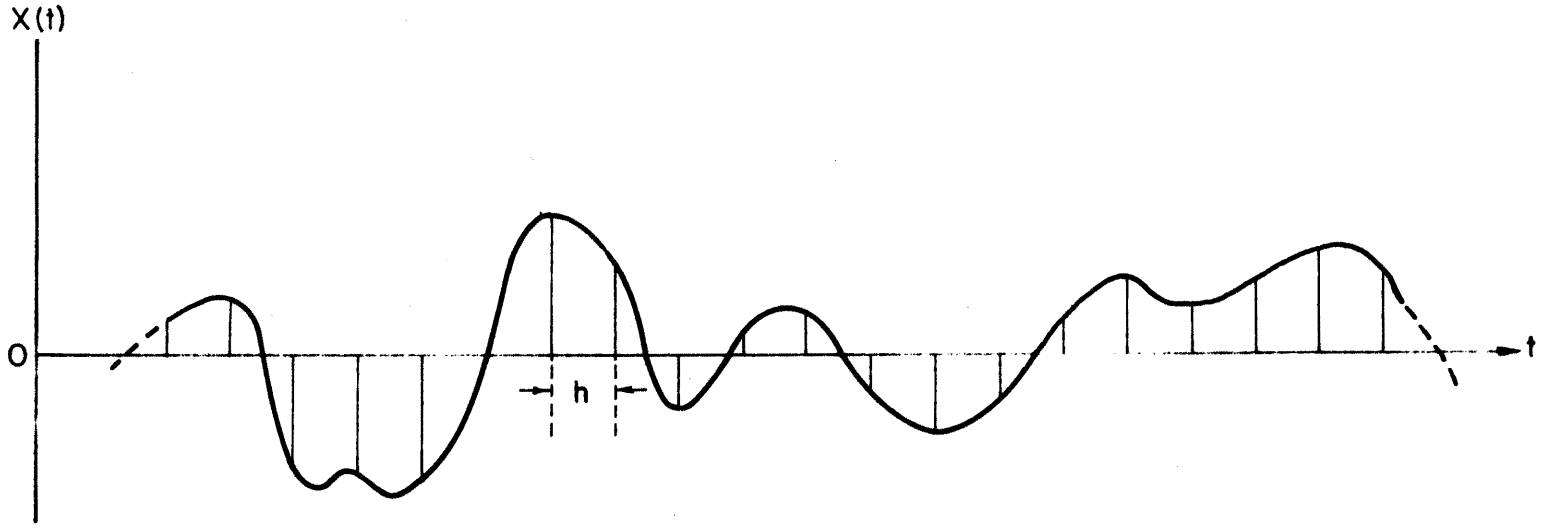

Figure 8. Sampling of continuous record. (Bendat and Piersol, 1966)

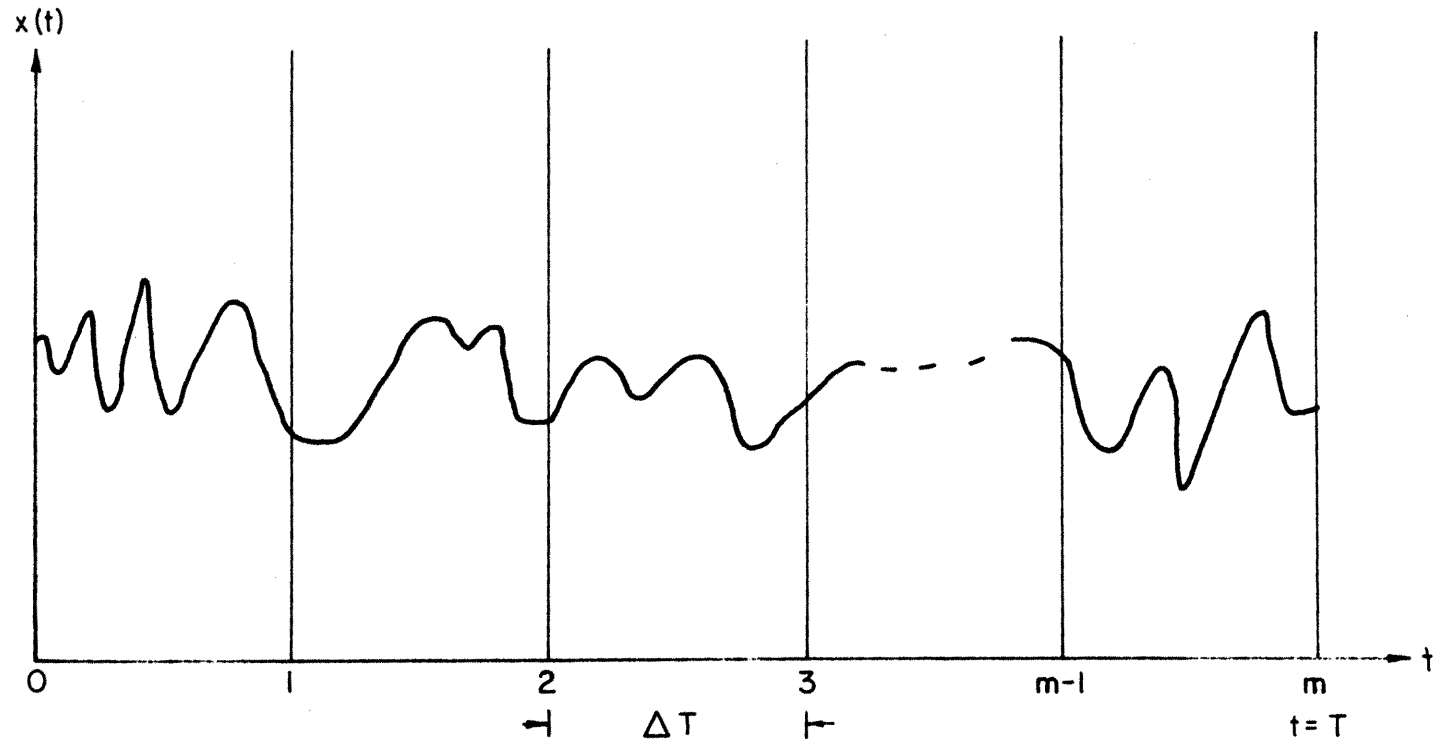

Figure 9. Continuous record of time T broken into m pieces of length ΔT.

$$\overline{\overline{(\,)}}_m = \frac{1}{T} \int_0^T (\,)\, dt \,,$$

$$= \frac{1}{m} \left\{ \frac{1}{\Delta T} \int_0^{\Delta T} (\,)\, dt + \ldots \frac{1}{\Delta T} \int_{(m-1)\Delta T}^{m\Delta T} (\,)\, dt \right\} \,,$$

$$= \frac{1}{m} \sum_{i=m}^{m} \overline{(\,)}_i \,. \qquad (13)$$

If a mean over m pieces has been computed and a mean of the next piece $(m + 1)$ has been calculated, the mean for $m + 1$ pieces is given by

$$\overline{\overline{(\,)}}_{m+1} = \frac{1}{m+1} \sum_{i=1}^{m+1} \overline{(\,)}_i \,,$$

$$= \frac{m}{m+1} \left\{ \frac{1}{m} \sum_{i=1}^{m} \overline{(\,)}_i + \frac{1}{m} \overline{(\,)}_{m+1} \right\} \,, \qquad (14a)$$

leading to the recursion formula for mean values:

$$\overline{\overline{(\,)}}_{m+1} = \frac{m}{m+1} \overline{\overline{(\,)}}_m + \frac{1}{m+1} \overline{(\,)}_{m+1} \,, \qquad (14b)$$

which requires only one additional storage space to accumulate the time average over the entire record.

Cross Correlations

The values to be correlated are the fluctuations about the mean value of the signal. If the mean of an individual piece is not zero, it is subtracted from each data point; therefore, the values $x(t)$ and $y(t)$ from beams A and B respectively are:

$$x(t) = X(t) - \overline{X(t)} \,,$$

$$y(t) = Y(t) - \overline{Y(t)} \,, \qquad (15)$$

where $X(t)$ and $Y(t)$ represent the actual data and $\overline{X(t)}$ and $\overline{Y(t)}$ represent the means over the piece.

The correlation $R_{xy}(\tau)$ is estimated by integrating over the delayed and undelayed sample functions. As shown in Figure 10, the time interval over the ith piece is from $(i-1)\Delta T + \tau$ and $i\Delta T$, where ΔT is the piece length. The cross correlation at a time delay τ over m pieces is given by

$$R_{xy}(\tau) = \frac{1}{m(\Delta T-\tau)} \sum_{i=1}^{m} \int_{(i-1)\Delta T+\tau}^{i\Delta T} x(t)y(t+\tau)\, dt ,$$

$$= \frac{1}{m} \sum_{i=1}^{m} [R_{xy}(\tau)]_i \quad . \tag{16}$$

The time lag is considered positive, since there is a positive translation of the signal along the time axis. For a negative translation, the time interval is from $(i-1)\Delta T$ and $i\Delta T - \tau$ and the cross correlation is

$$R_{xy}(-\tau) = \frac{1}{m(\Delta T-\tau)} \sum_{i=1}^{m} \int_{(i-1)\Delta T}^{i\Delta T-\tau} x(t)y(t-\tau)\, dt . \tag{17a}$$

Set $t' = t - \tau$. Then

$$R_{xy}(-\tau) = \frac{1}{m(\Delta T-\tau)} \sum_{i=1}^{m} \int_{(i-1)\Delta T-\tau}^{i\Delta T} x(t' + \tau)y(t')\, dt' . \tag{17b}$$

The above expression resembles positive lags if x and y are switched. For comparison purposes, the normalized cross correlation is

$$\hat{R}_{xy}(\tau) = \frac{1}{m} \sum_{i=1}^{m} \left\{ \frac{R_{xy}(\tau)}{[R_x(o)]^{1/2}[R_y(o)]^{1/2}} \right\}_i \tag{18}$$

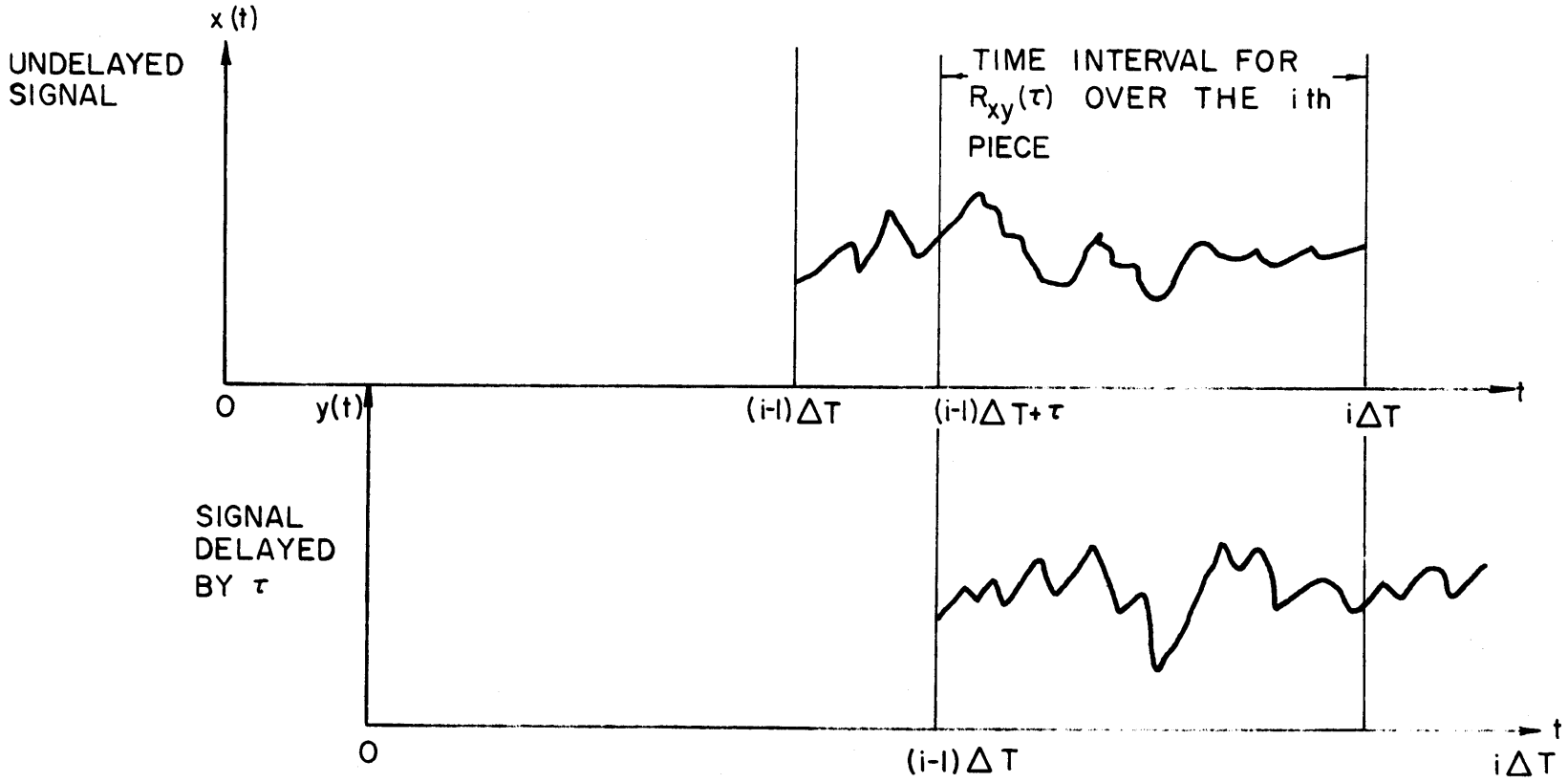

Figure 10. Time interval for the piecewise correlation of signals $x(t)$ and $y(t)$ at a time delay τ.

As stated in the section on analog data reduction, the time lag corresponding to the maximum correlation should be the transit time corresponding to the dominant wind speed or

$$v = \xi/\tau_m \ , \tag{19}$$

where ξ is the beam separation and τ_m is the delay time corresponding to the maximum correlation. For zero beam separations, the maximum correlation occurs at zero time lag.

RESULTS

Six experiments with beam separations ranging from 41.5 meters to 224 meters are discussed. Figures 11, 13, 15, 17, 19, and 21 show a top view of the field setup. The date the experiment was performed is included, as well as the starting and ending times, sky condition, height of the minimum beam separation, wind detection range, and dominant wind speed.

Figures 12, 14, 16, 18, 20, and 22 show the analog and digital correlations and Table 1 provides a summary of the maximum correlations and computed wind speeds for each run as well as the dominant wind speeds from cup anemometers. Runs 1, 2, and 3 compare favorably with the anemometer speeds. Run 1 had a dominant wind speed of -4.1 mps (taken as negative, since the wind is detected by the second beam first). For a beam spearation of 115.5 meters, a maximum correlation at a time lag of -28 seconds is expected. Both analog and digital correlations show the maximum value very close to the expected time lag (Figure 12). Run 2 had a dominant wind speed of -6.8 mps and a beam separation of 41.5 meters. A maximum correlation at a time lag of -6 seconds would be expected. The analog and digital correlations showed peaks at time lags of -7 and -5.5 seconds respectively (Figure 14) resulting in computed wind speeds of -5.9 and -7.5 mps respectively. Run 3 had a higher wind speed (-11 mps) than Runs 1 and 2. For a beam separation of 99 meters, a maximum correlation at a time delay of -9 seconds would be expected. The analog and digital correlations peaked at time delays of -7.5 and -11 seconds respectively resulting in computed speeds of -13.2 and -9 mps respectively (Figure 16). Runs 4, 5, and 6 did not compare as favorably to the anemometer results as Runs 1, 2, and 3. Runs 4 and 5 had long

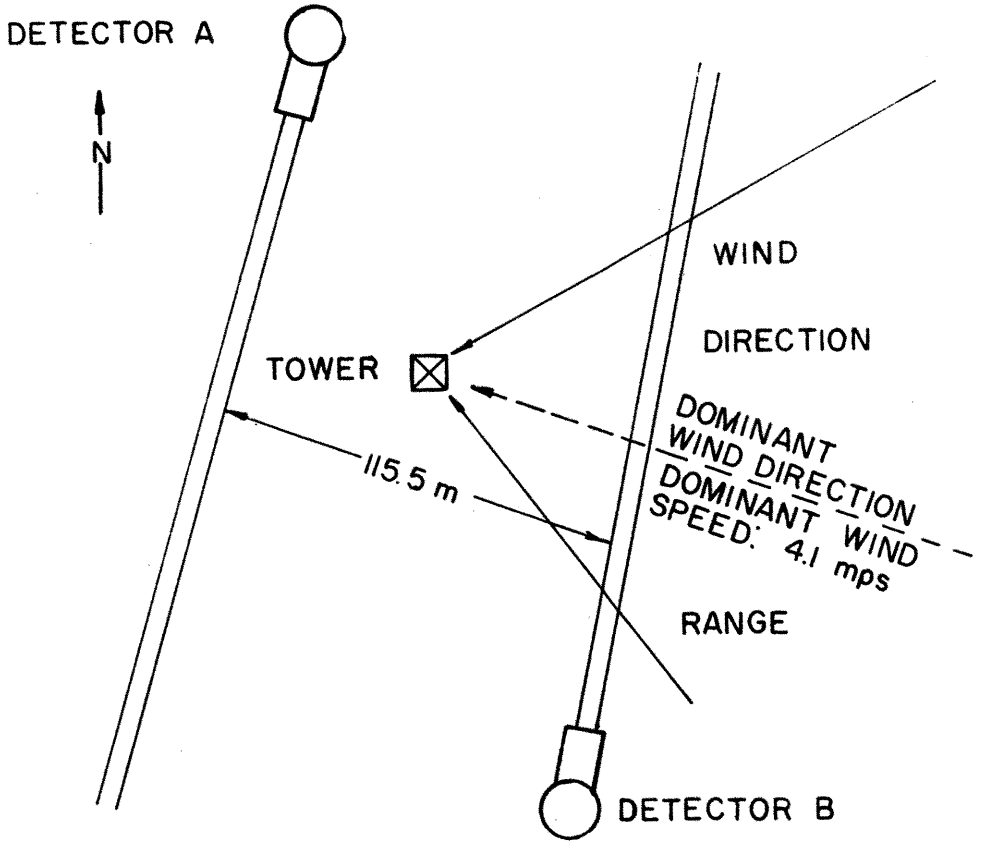

DATE OF RUN: 3 JANUARY 1968
STARTING TIME: 1101 (MST)
ENDING TIME: 1203 (MST)
SKY CONDITION: CLEAR
HEIGHT OF MINIMUM BEAM SEPARATION: 61 m

Figure 11. Test arrangement and conditions for Run 1.

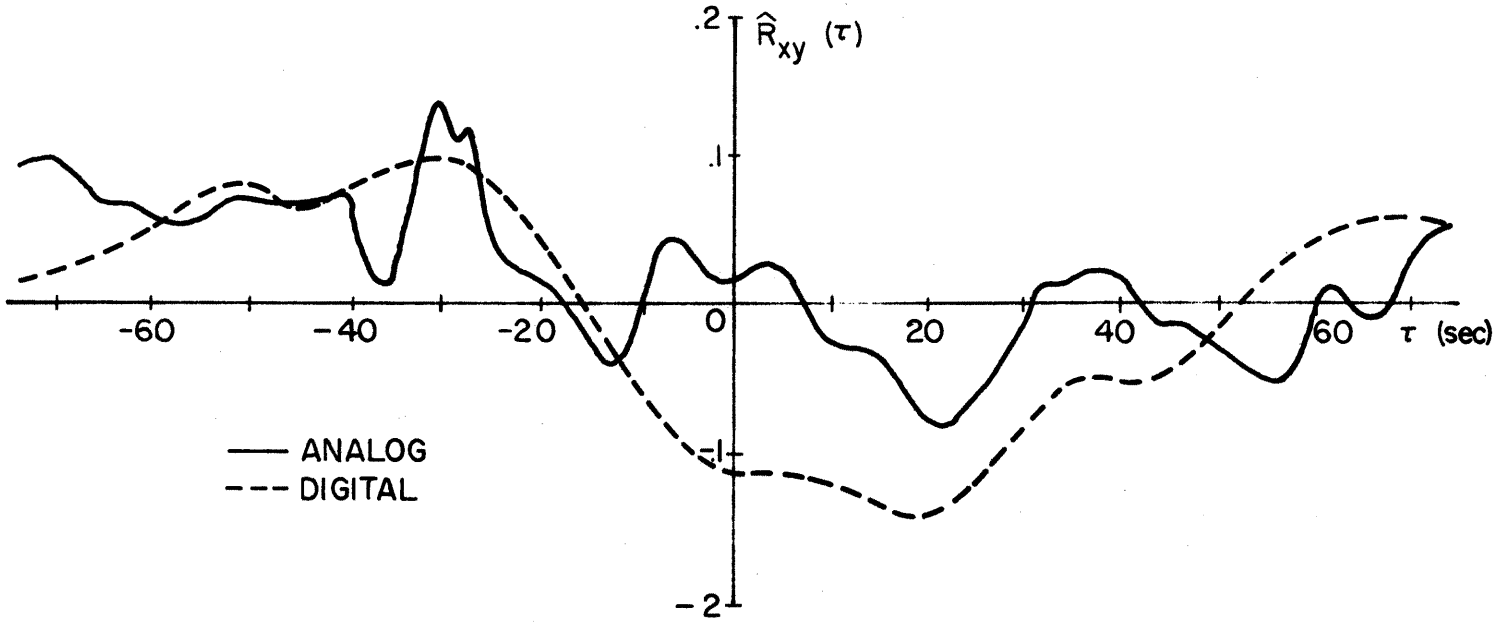

Figure 12. Analog and digital correlations for Run 1.

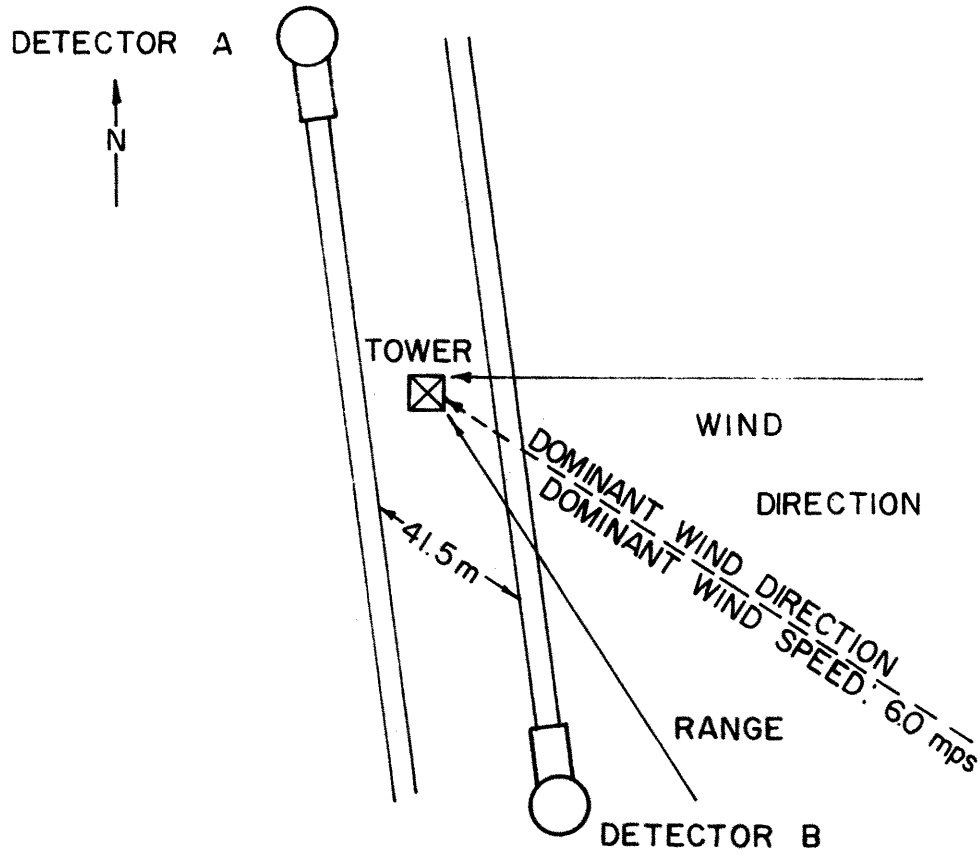

DATE OF RUN: 3 JANUARY 1968
STARTING TIME: 1227 (MST)
ENDING TIME: 1336 (MST)
SKY CONDITION: CLEAR
HEIGHT OF MINIMUM BEAM SEPARATION: 61 m

Figure 13. Test arrangement and conditions for Run 2.

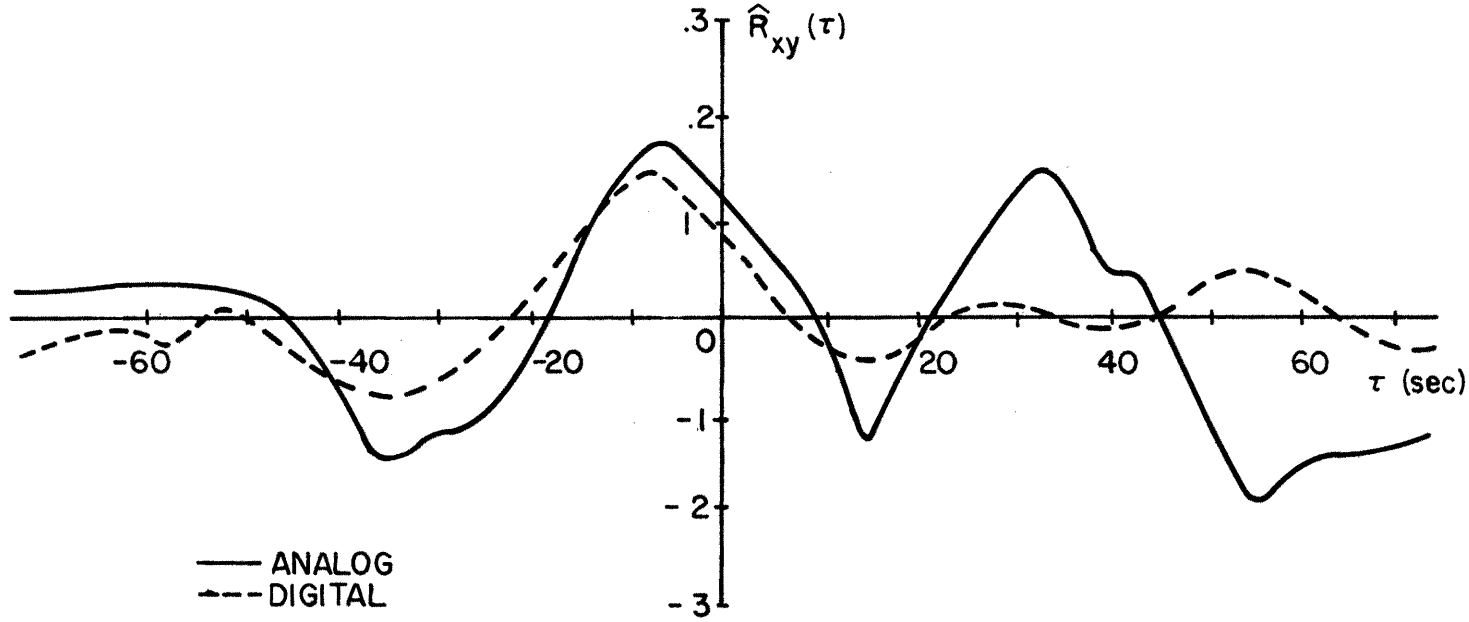

Figure 14. Analog and digital correlations for Run 2.

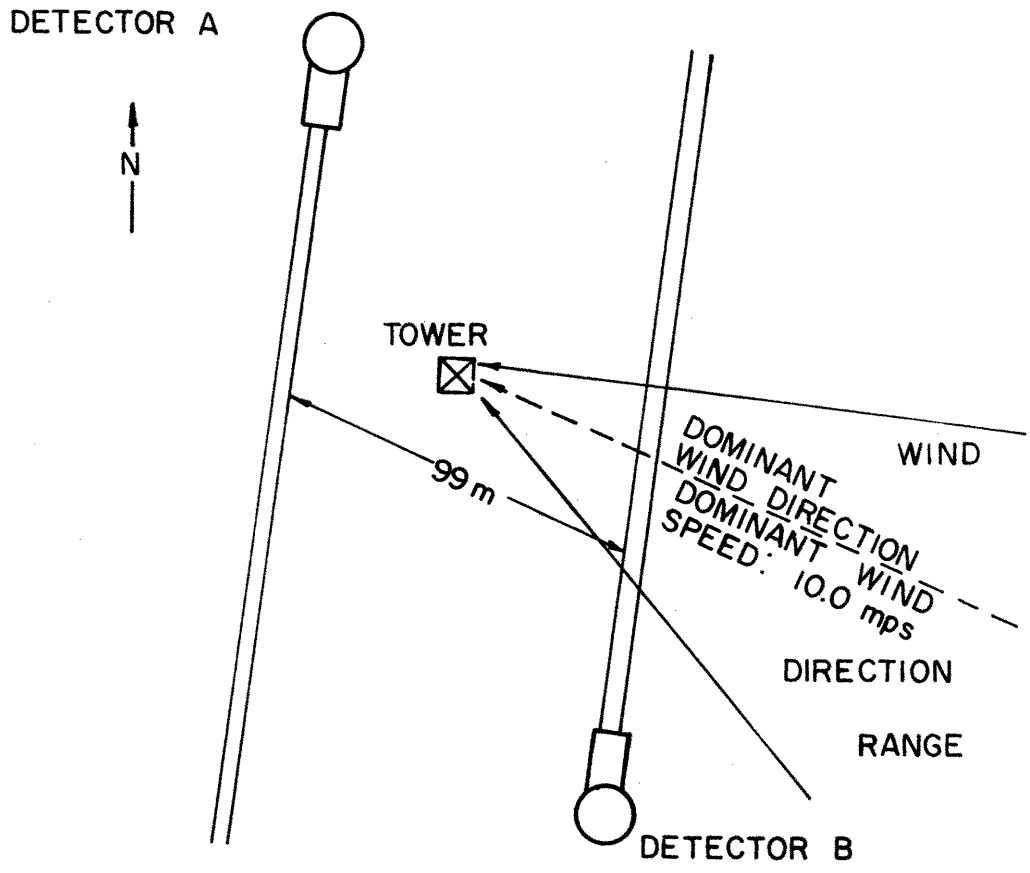

DATE OF RUN: 3 JANUARY 1968
STARTING TIME: 1303 (MST)
ENDING TIME: 1449 (MST)
SKY CONDITION: CLEAR
HEIGHT OF MINIMUM BEAM SEPARATION: 61 m

Figure 15. Test arrangement and conditions for Run 3.

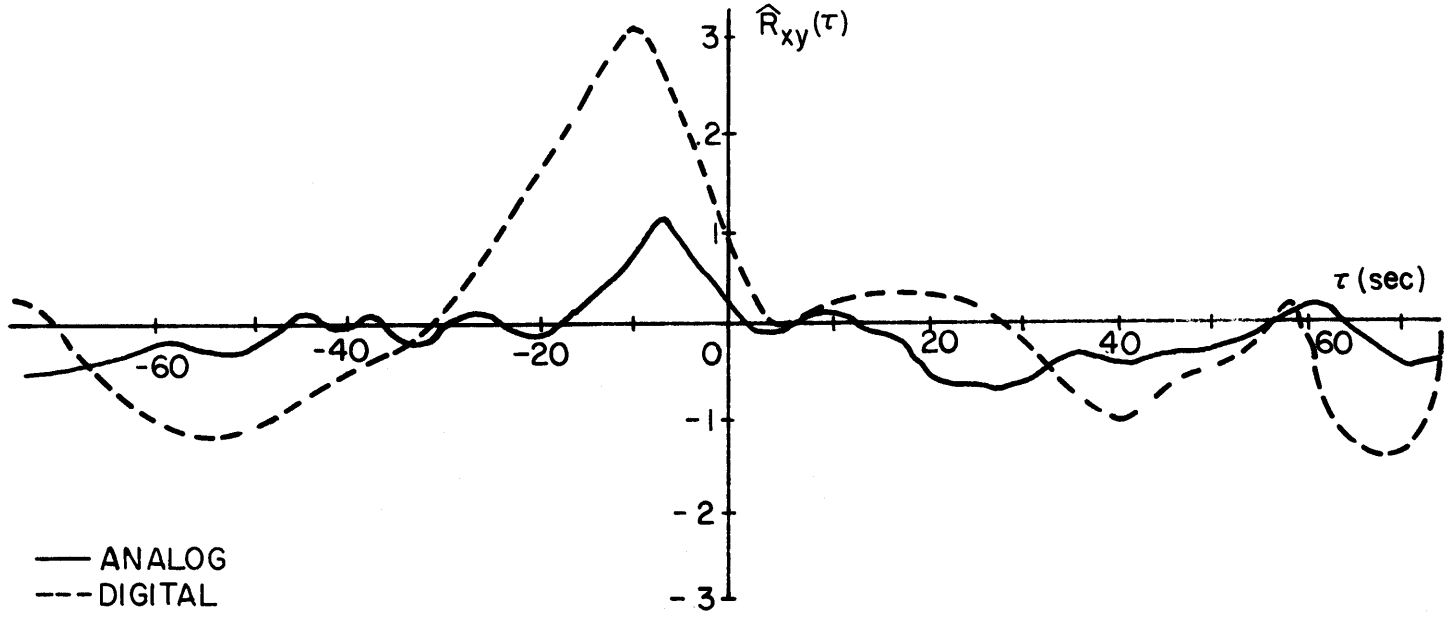

Figure 16. Analog and digital correlations for Run 3.

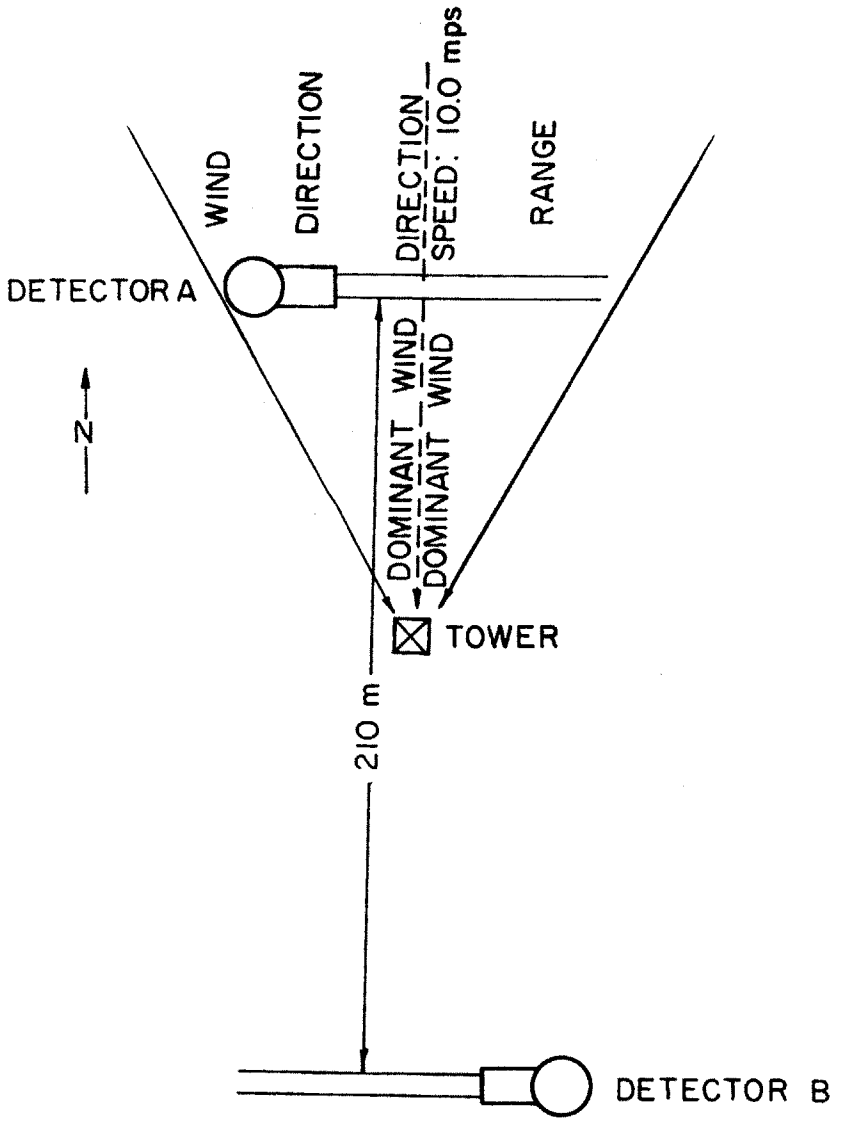

DATE OF RUN: 22 MARCH 1968
STARTING TIME: 1417 (MST)
ENDING TIME: 1607 (MST)
SKY CONDITION: CLEAR
HEIGHT OF MINIMUM BEAM SEPARATION: 61m

Figure 17. Test arrangement and conditions for Run 4.

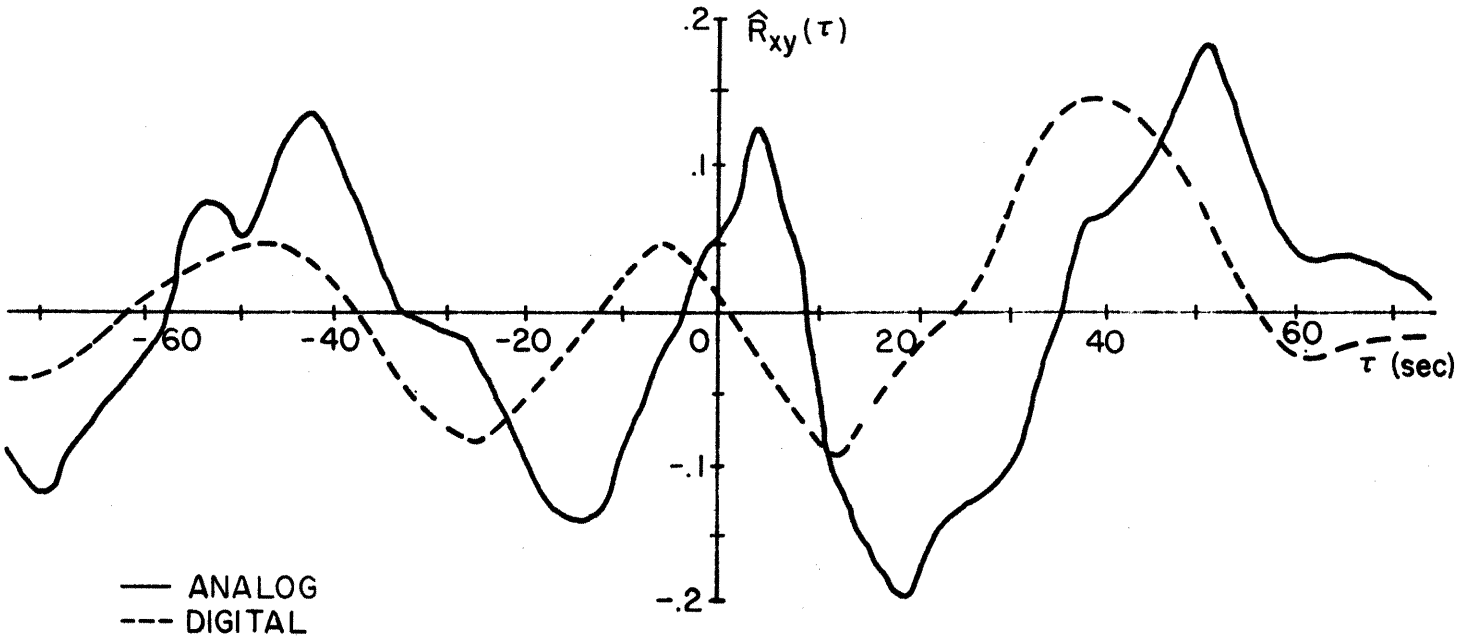

Figure 18. Analog and digital correlations for Run 4.

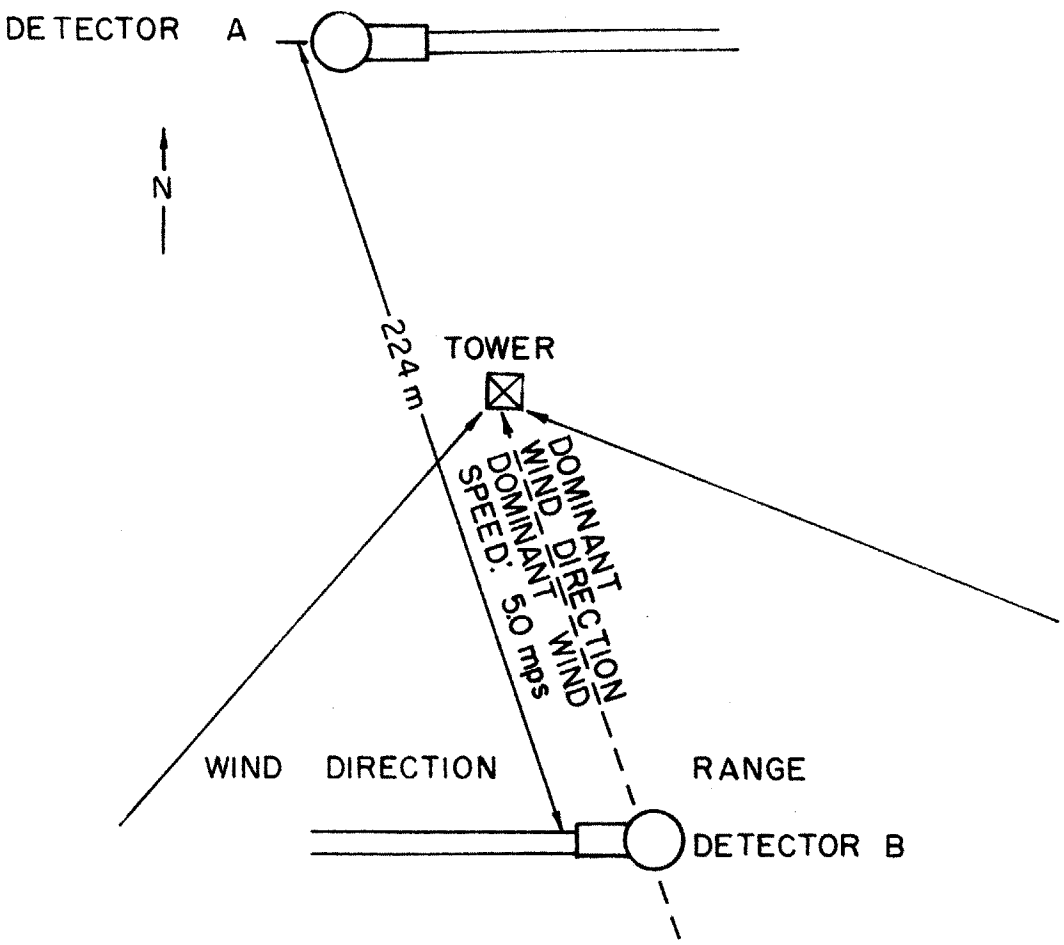

DATE OF RUN: 25 MARCH 1968
STARTING TIME: 1444 (MST)
ENDING TIME: 1516 (MST)
SKY CONDITION: CLEAR
HEIGHT OF MINIMUM BEAM SEPARATION: 61m

Figure 19. Test arrangement and conditions for Run 5.

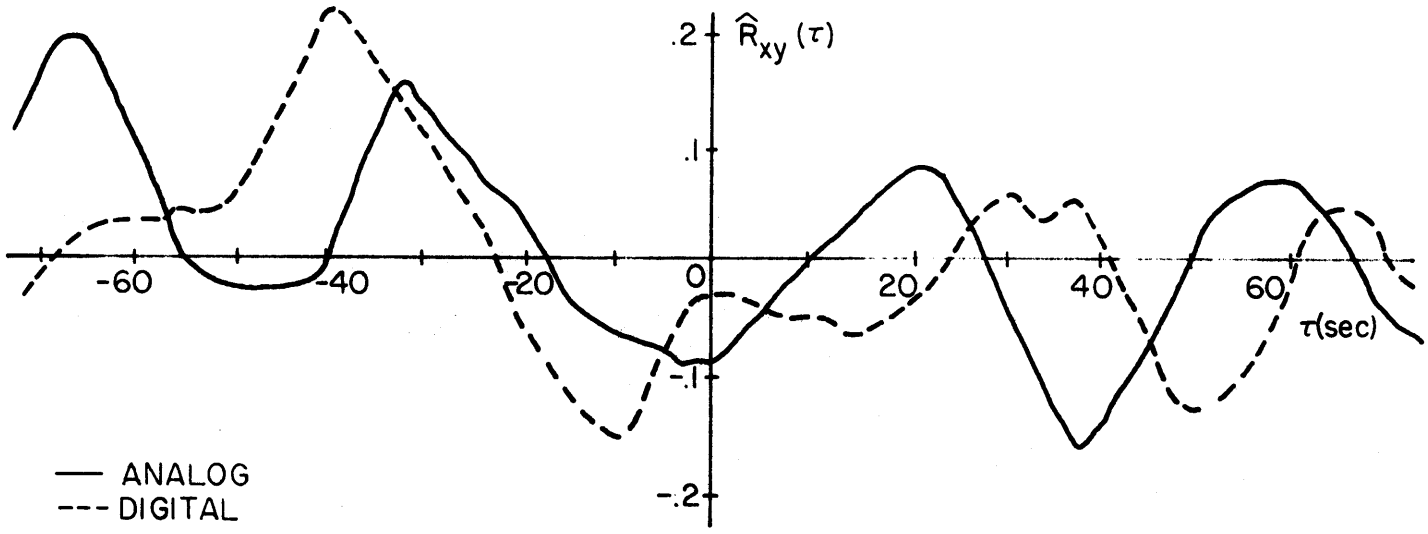

Figure 20. Analog and digital correlations for Run 5.

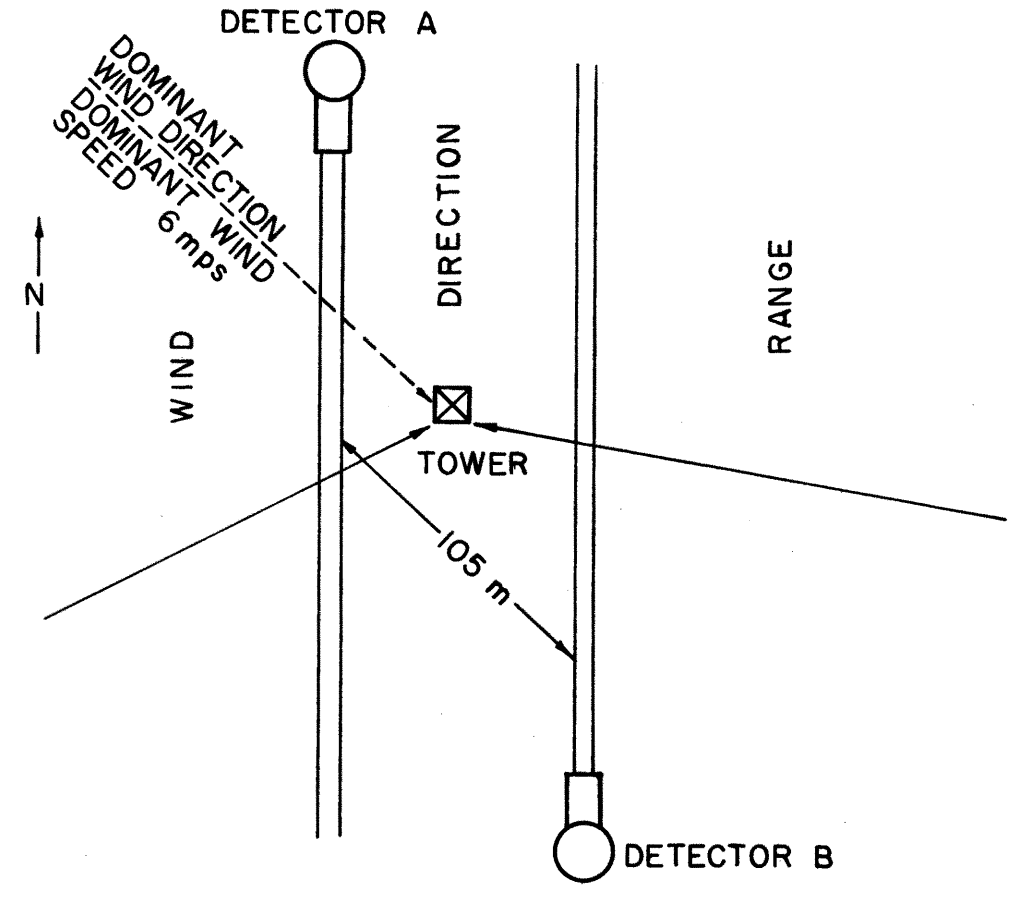

DATE OF RUN: 26 MARCH 1968
STARTING TIME: 1144 (MST)
ENDING TIME: 1358 (MST)
SKY CONDITION: OVERCAST
HEIGHT OF MINIMUM BEAM SEPARATION: 2 m

Figure 21. Test arrangement and conditions for Run 6.

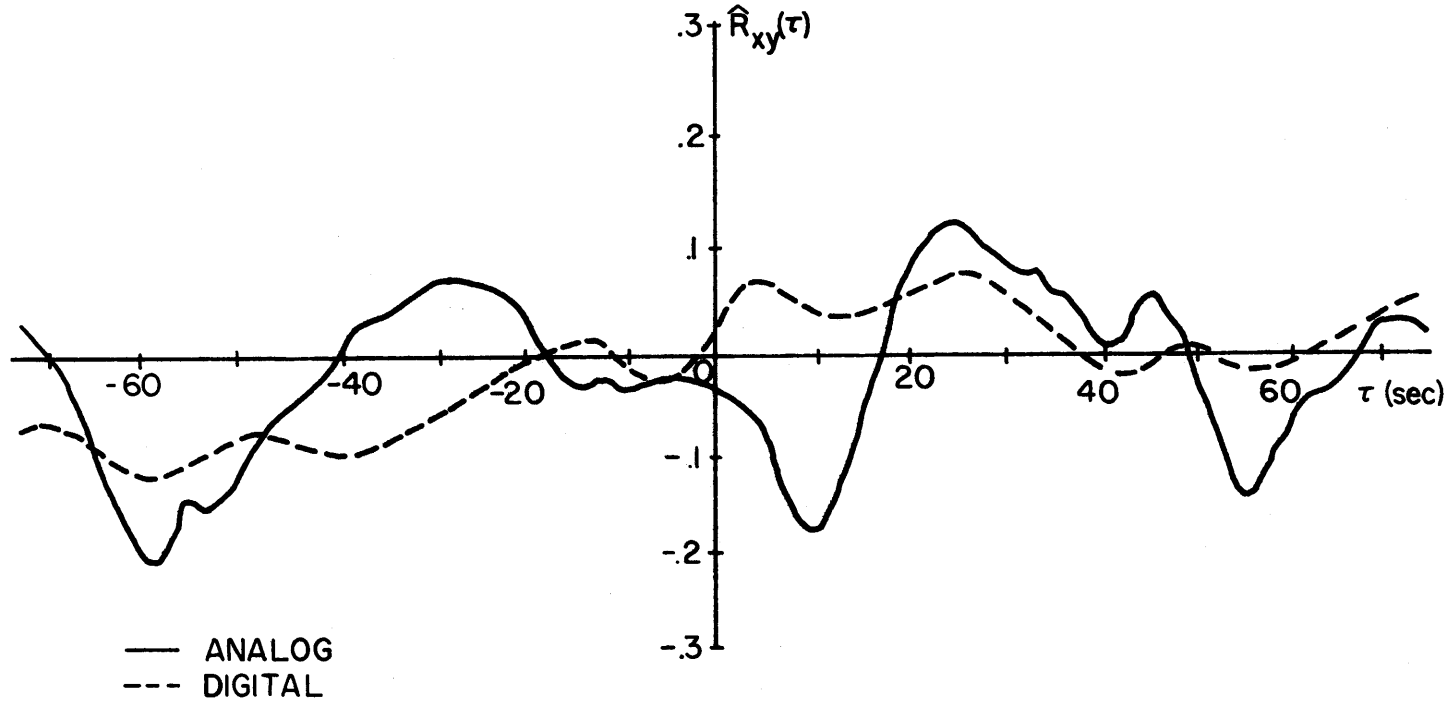

Figure 22. Analog and digital correlations for Run 6.

Table 1. Summary of Cross Beam Results for Runs 1-6.

RUN		ANALOG			DIGITAL			ANEMOMETER	
	ξ (m)	$R_{xy}(\tau)$	τ (sec)	v (mps)	$R_{xy}(\tau)$	τ (sec)	v (mps)	τ (sec)	v (mps)
1	115.5	.14	-28.5	-4.1	.10	-28.0	-4.1	-28.0	-4.1
2	41.5	.18	-7.0	-5.9	.16	-5.5	-7.5	-6.0	-6.8
3	99.0	.11	-7.5	-13.2	.33	-11.0	-9.0	-9.0	-11.0
4	210.0	.17	52.0	4.0	.14	39.5	5.2	21.0	10.0
5	224.0	.19	-66.5	-3.4	.21	-39.0	-5.8	-45.0	-5.0
6	105.0	.13	25.0	4.2	.08	27.0	3.9	15.5	6.7

BASIC DIFFERENCES BETWEEN ANALOG AND DIGITAL DATA REDUCTION

Analog	Digital
Original data	Digitized data
Entire record examined at once	Record broken into pieces
Curves not exactly reproducible	Reproducible curves
All signals included in data reduction	Obvious bad signals eliminated
Only correlations available	Information besides correlations available

separations (210 and 224 meters respectively). For Run 4, the computed wind speeds from the analog and digital correlations as shown in Figure 18 (4 mps at a time lag of 52 seconds from analog results and 5.2 mps at a time lag of 39.5 seconds from digital results) were roughly half the anemometer speed (10 mps). Run 5 had an anemometer speed of -5 mps. The digital correlation (Figure 20) had a maximum correlation at a time delay of -39 seconds resulting in a computed wind speed of -5.8 mps, which shows a fair agreement with the anemometer speed. The analog correlation showed a peak at a time delay of -66.5 seconds or a computed wind speed of -3.2 mps, which was about 36% less than the anemometer speed. Run 6 differed from the previous runs in two respects. First, the experiment was conducted under cloudy skies. Second, the beams were parallel to the ground, making the minimum beam separation only two meters above the ground. This was done to keep amplifier saturation at a minimum. The beam separation was 105 meters and the dominant anemometer speed was 6.7 mps. The analog and digital correlations peaked at time delays of 25 and 27 seconds respectively resulting in computed speeds of 4.2 and 3.9 mps respectively.

Since Run 6 was performed under cloudy conditions and the beams were close to the ground, the possibility existed that the energy detected by both beams had dominant frequencies different from the previous runs. By use of a 1/10 octave band width spectrum analyzer, the energy distribution at different frequencies can be obtained. By dividing the energy at a given frequency by the frequency (which is proportional to the band width), the spectral density $S(f)$ is obtained. For comparison purposes, the spectral density is normalized by dividing $S(f)$ by the total energy estimate e_T^2, or

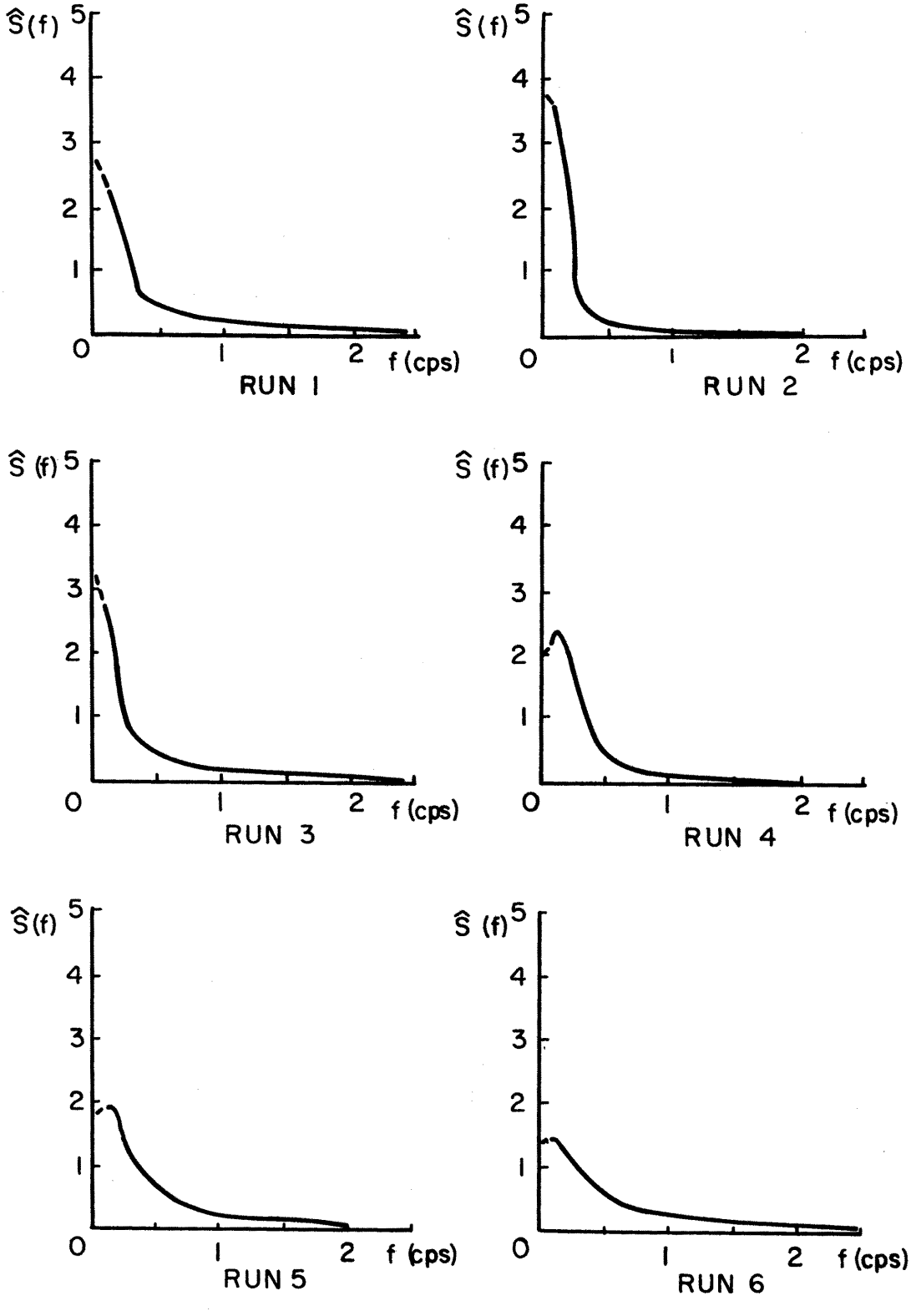

Figure 23. Power spectral density for Runs 1-6 (Beam A).

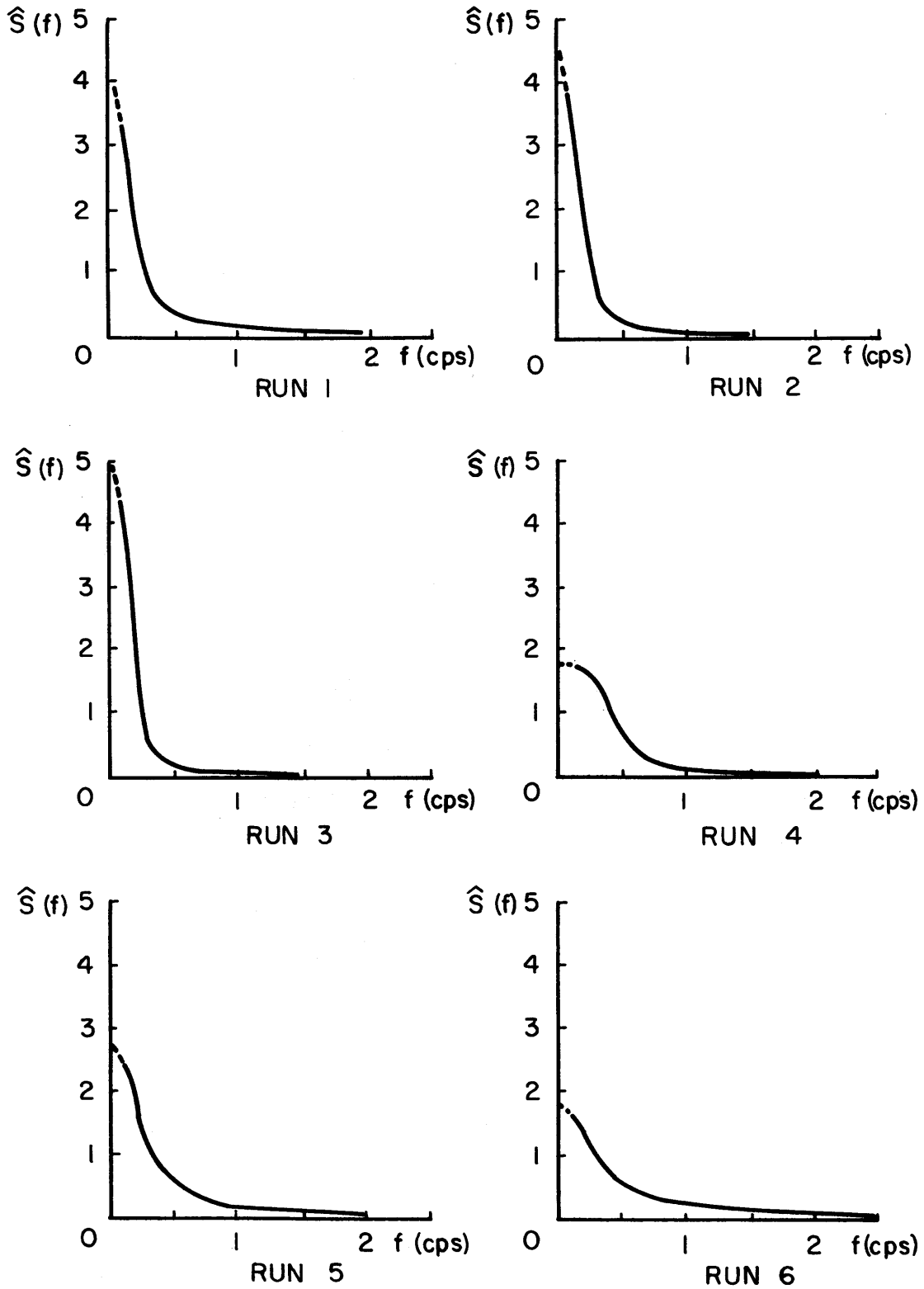

Figure 24. Power spectral density for Runs 1-6 (Beam B).

$$\hat{S}(f) = \frac{e^2}{e_T^2 f} \quad ,$$

$$= \frac{S(f)}{e_T^2} \quad , \tag{20}$$

where e^2 is the energy estimate at a given frequency f. Plots of $\hat{S}(f)$ vs. frequency for each run are shown in Figures 23-24 (see appendix for original data and computed values of $\hat{S}(f)$). Only the energy in this frequency range would be considered. The area under the curves in Figures 23-24 gives an estimate of the total energy for each run. By finding the area for frequencies less than or equal to .333 cps only, the percentage of energy below .333 cps can be obtained. The results for each run are summarized in Table 2. Only Run 6 shows that more than half of the total energy occurs at frequencies above .333 cps. By Eq. (6), the upper frequency can be increased by using shorter time lags. Analyses were done on each run using the shorter time lag ranges. For Runs 1-5, the results were practically the same, but the results of Run 6 were improved. The analog and digital correlations showed peaks at time delays of 21 and 20.5 seconds respectively (Figure 25) resulting in computed wind speeds of 5.0 and 5.1 mps respectively. The computed speeds are closer to the anemometer speed of 6.7 mps than the original computed wind speeds of 4.2 mps (analog) and 3.9 mps (digital). It would appear that a suitable time lag range is one which will result in a frequency range containing at least half of the total energy.

Since Runs 4 and 5 had long separations, the possibility existed that there were signals, which were not common to both beams. All experiments were analyzed assuming that the signals common to both beams

Table 2. Fraction of Energy at Frequencies Below .333 CPS for Runs 1-6.

Run	Percentage of Energy Below .333 CPS	
	Beam A	Beam B
1	59	65
2	75	85
3	59	87
4	70	55
5	55	65
6	43	47

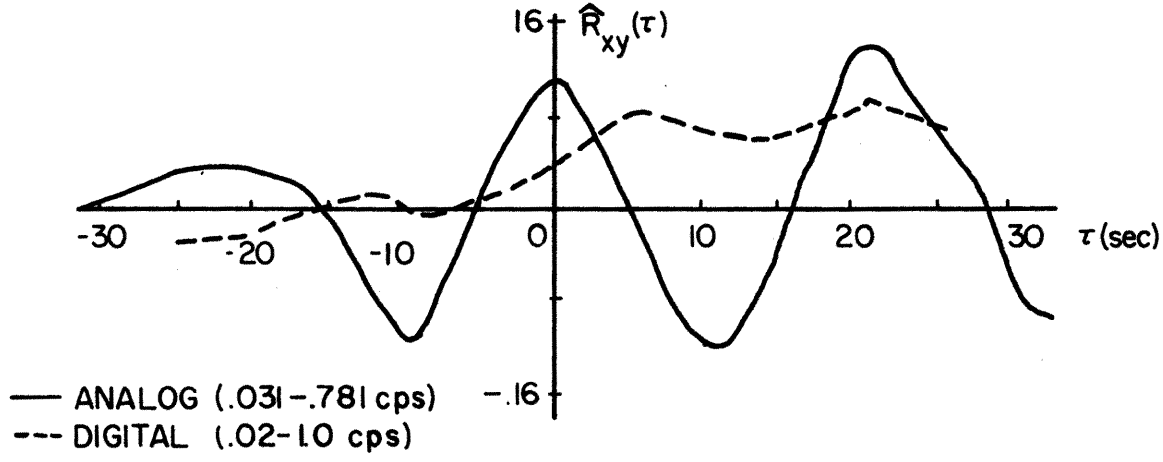

Figure 25. Analog and digital correlations for Run 6 at higher frequencies and shorter time lag ranges.

yielded positive correlations. However, it was suggested by Sandborn that when the aerosols travel from one beam to another, light may be scattered into one beam and away from the other, yielding a negative correlation caused by the common signal. To determine whether there is a dominance of positive or negative correlations, the following quantities are defined:

$$x_+ = x, \quad x \geq 0$$
$$= 0, \quad x \leq 0, \tag{21}$$

$$x_- = 0, \quad x \geq 0$$
$$= x, \quad x \leq 0 \ . \tag{22}$$

The quantities y_+ and y_- are defined in a similar manner. For each of the six experiments, the following correlations were computed (Figures 26-31):

$$R_{x+y+}(\tau) = \frac{1}{T}\int_0^T x_+(t)y_+(t+\tau)\,dt,$$

$$R_{x+y-}(\tau) = \frac{1}{T}\int_0^T x_+(t)y_-(t+\tau)\,dt,$$

$$R_{x-y+}(\tau) = \frac{1}{T}\int_0^T x_-(t)y_+(t+\tau)\,dt,$$

$$R_{x-y-}(\tau) = \frac{1}{T}\int_0^T x_-(\tau)y_-(t+\tau)\,dt. \tag{23}$$

There was a dominance of positive correlations for the experiments, which provided wind speeds comparable to anemometer speeds (Runs 1, 2, 3, and 6). $R_{x_-y_-}(\tau)$ was the dominant correlation for Runs 1-3 and $R_{x_+y_+}(\tau)$ was dominant for Run 6. Runs 4 and 5 did not have a dominant set of

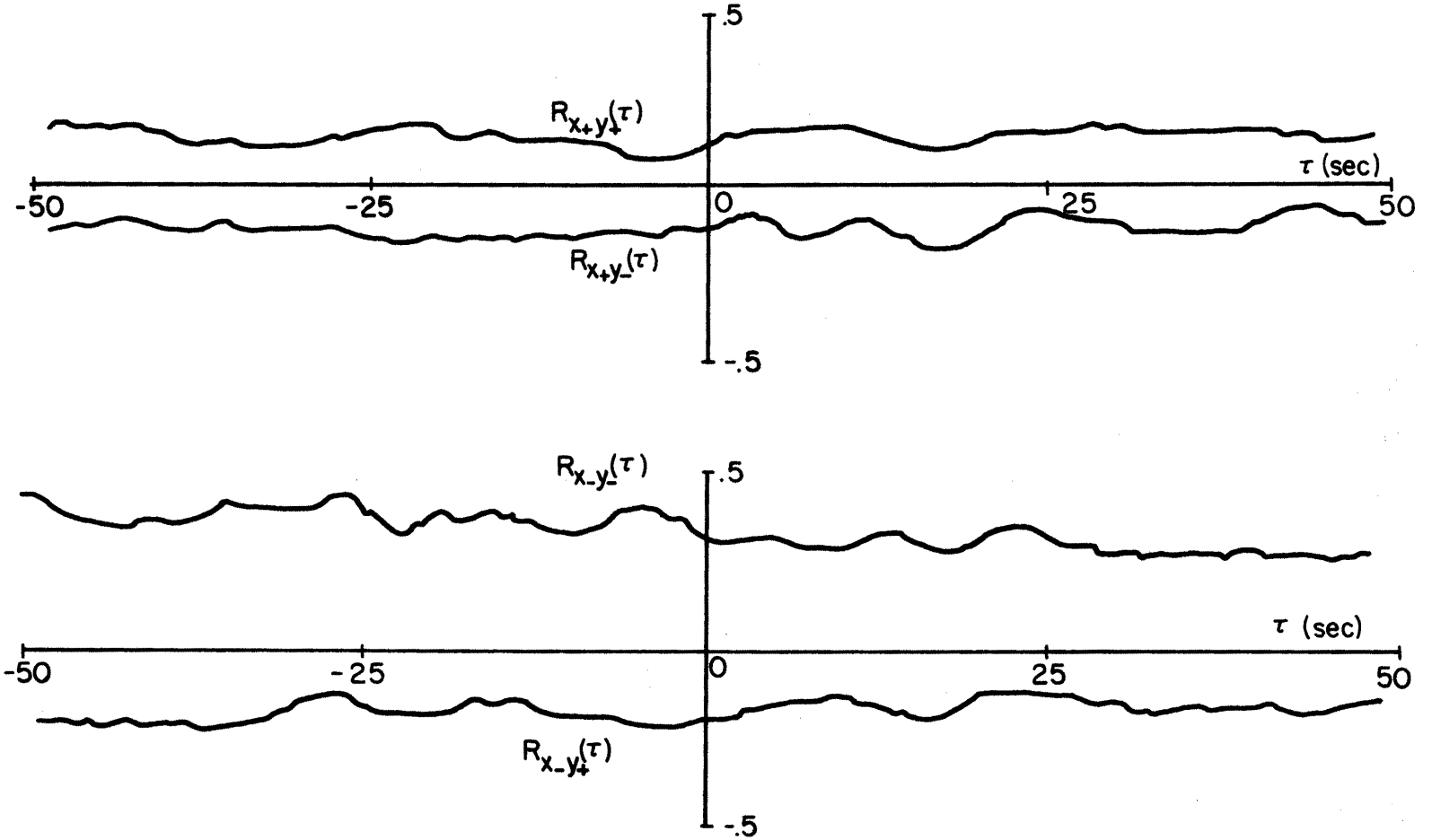

Figure 26. Rectified correlations for Run 1.

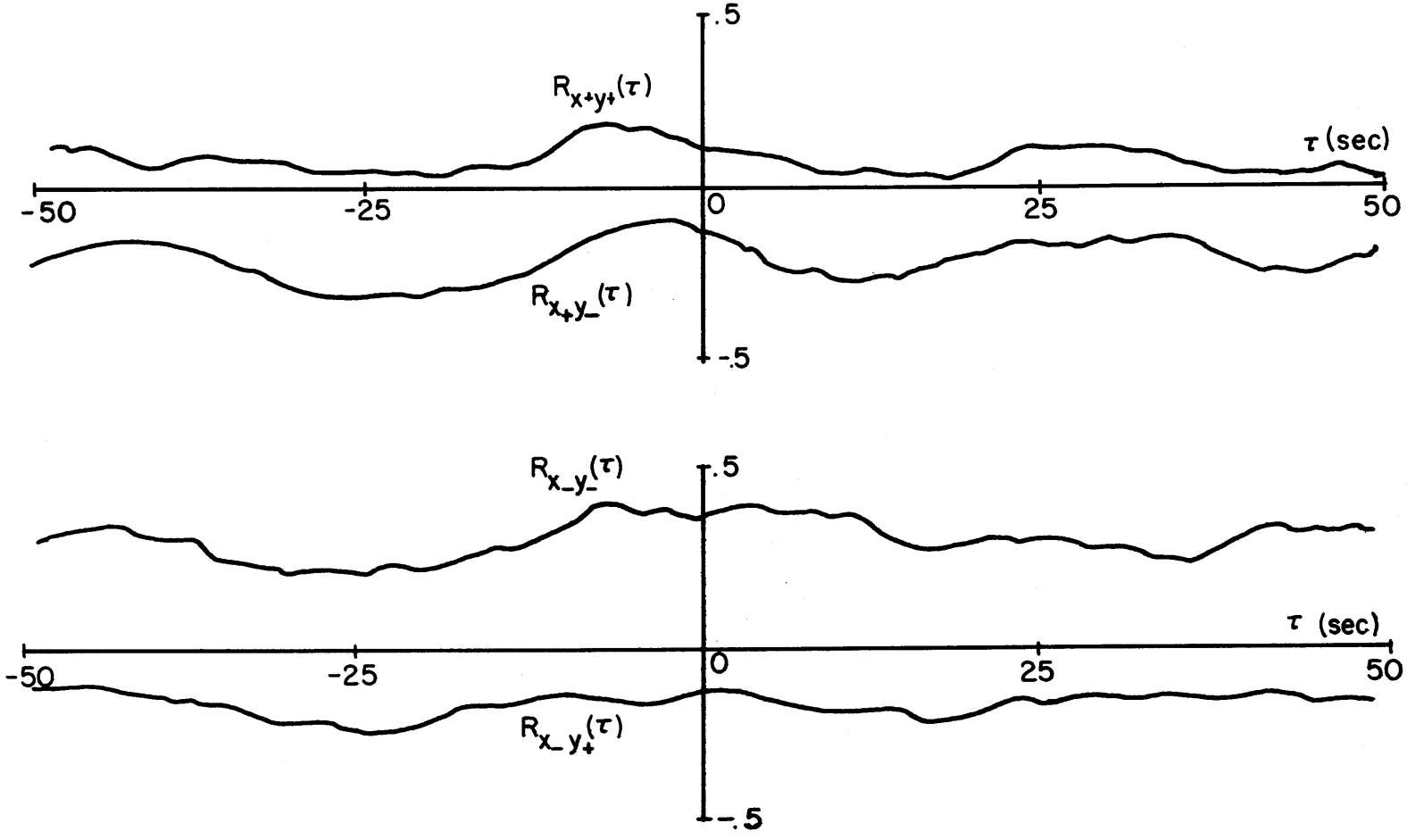

Figure 27. Rectified correlations for Run 2.

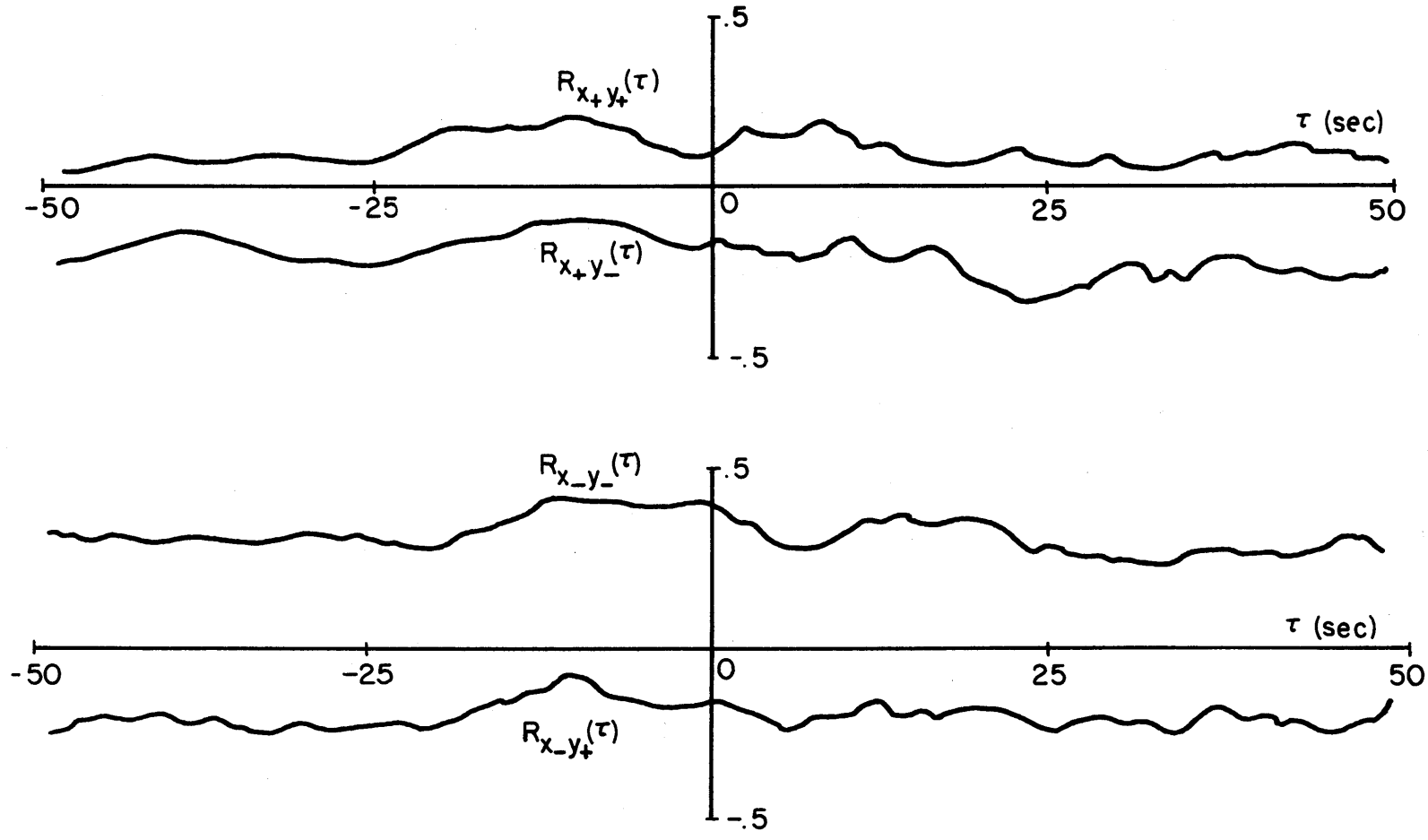

Figure 28. Rectified correlations for Run 3.

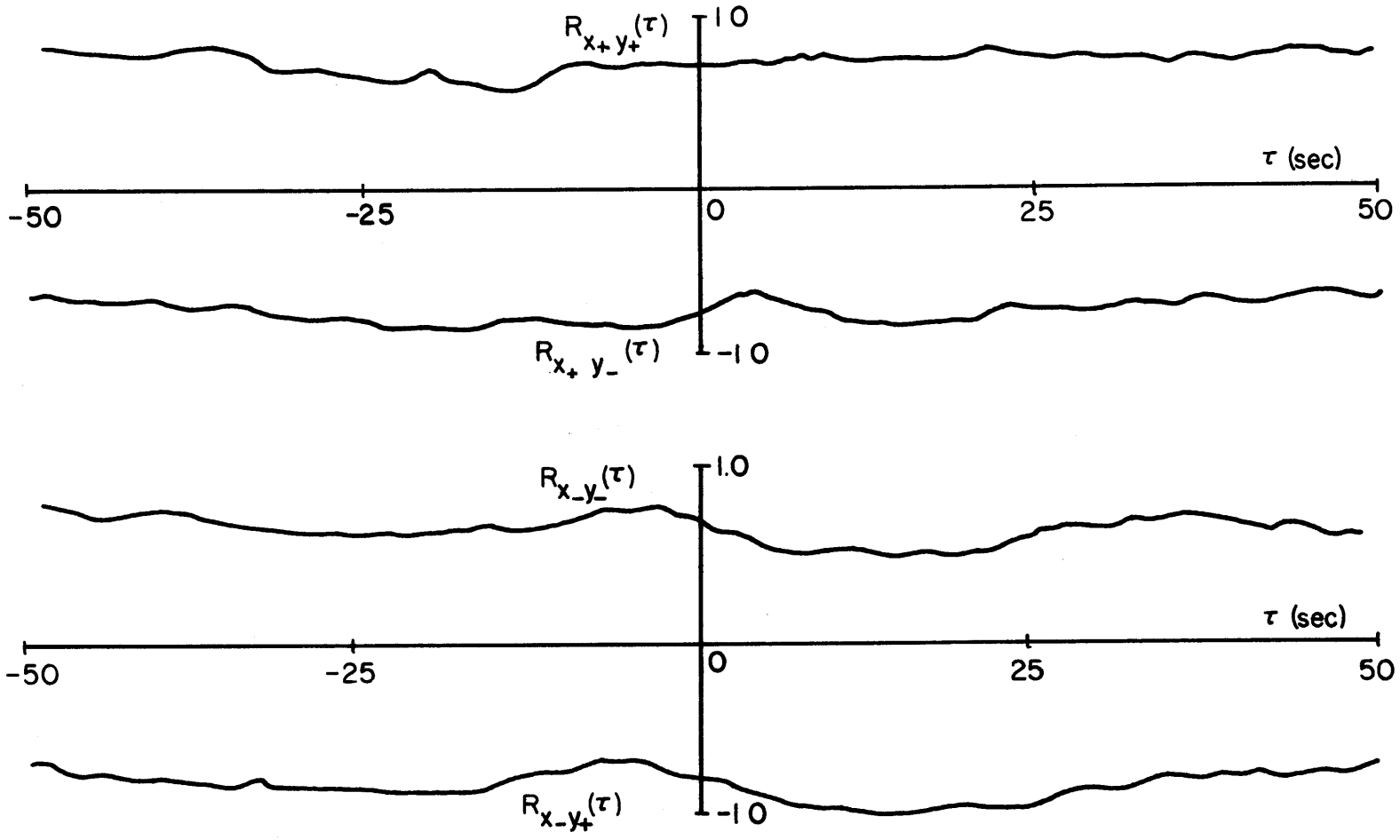

Figure 29. Rectified correlations for Run 4.

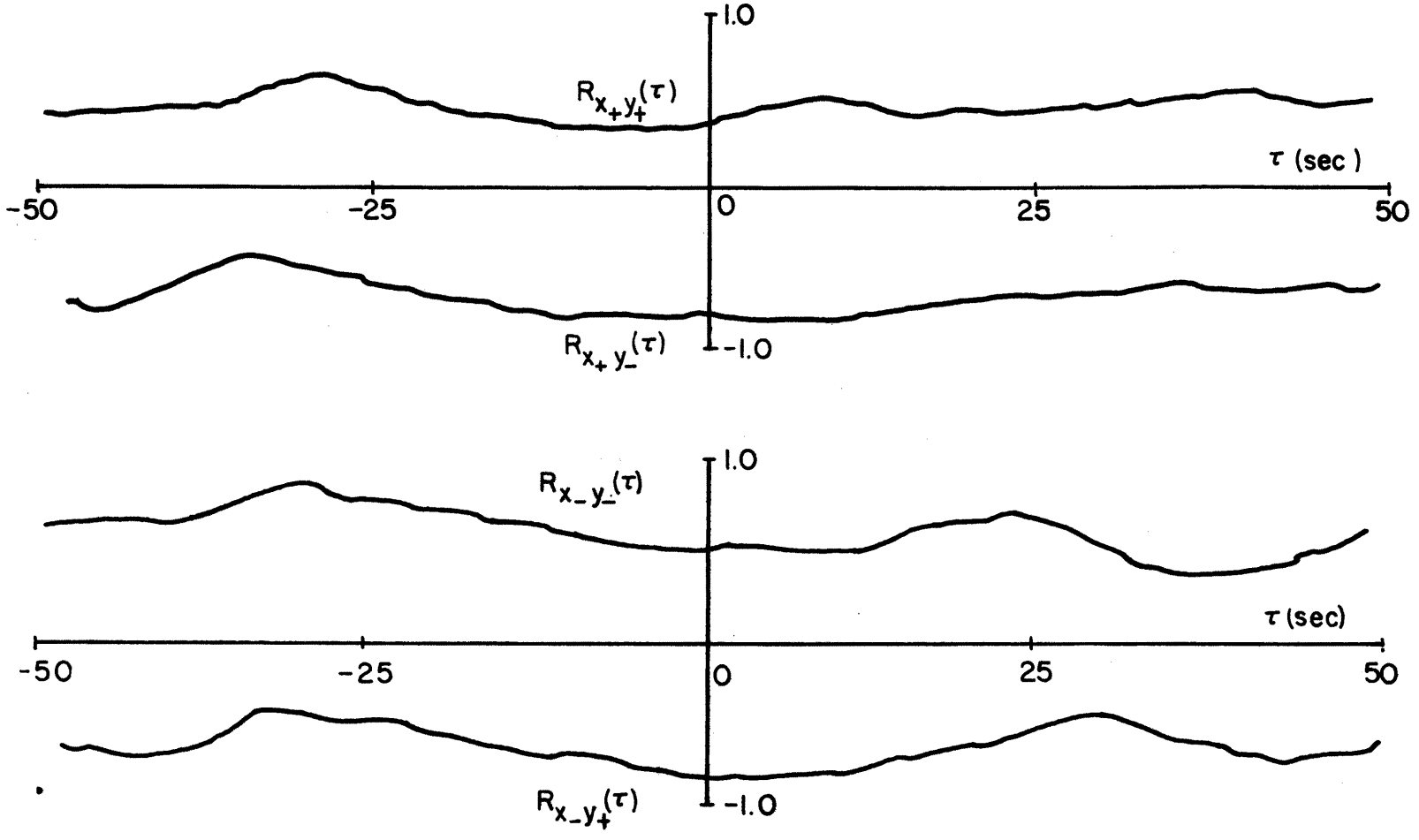

Figure 30. Rectified correlations for Run 5.

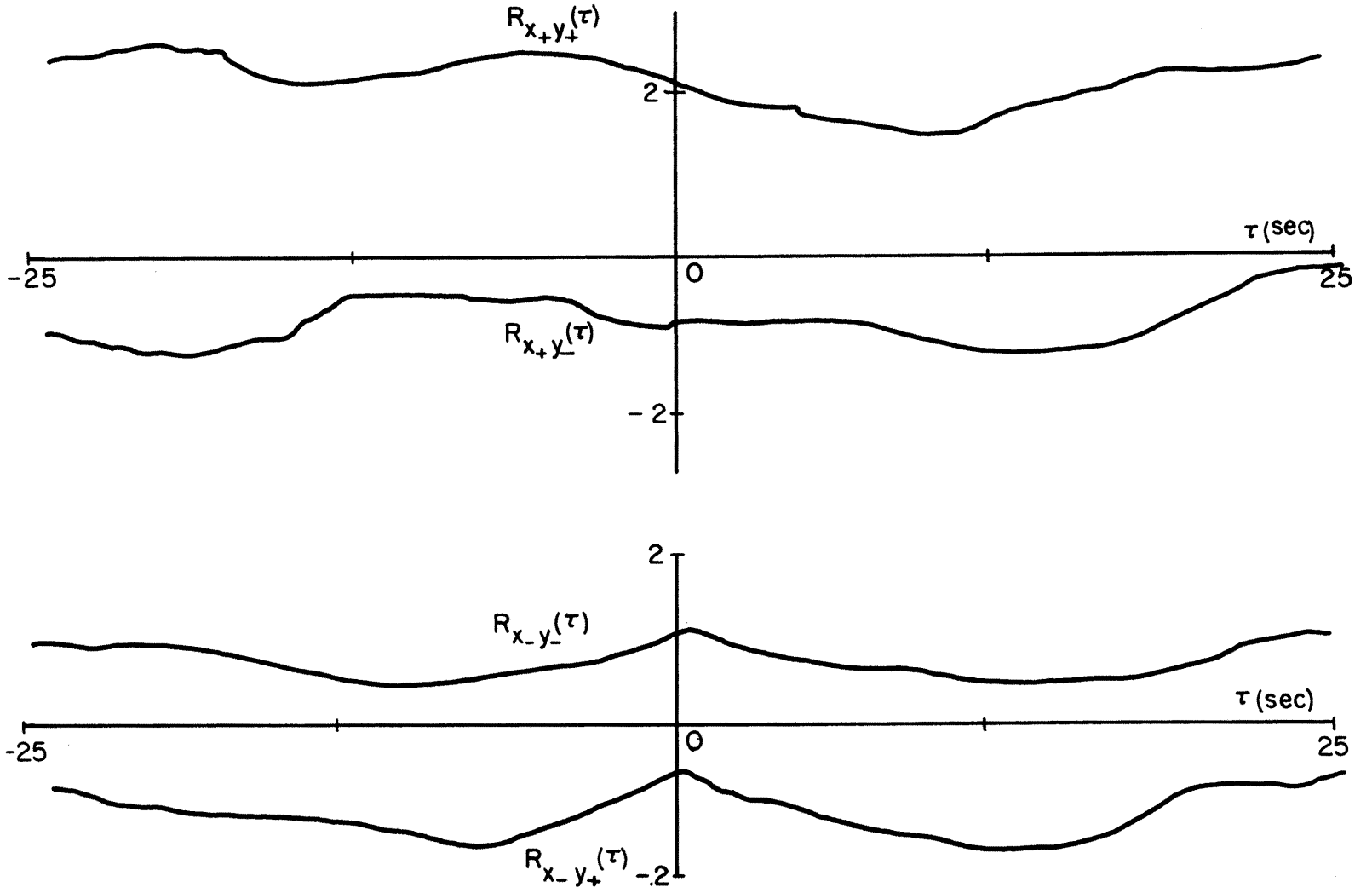

Figure 31. Rectified correlations for Run 6.

correlations. This means that if there were signals common to both beams, there was an equal likelihood of the correlations' being positive or negative. No experiments were found to have a dominance of negative correlations.

It would appear that the minimum requirements for wind detection by the cross beam technique should be dominant positive correlations and time lag ranges chosen so that at least half of the total energy is considered.

SUMMARY AND CONCLUSIONS

The primary aim of this investigation was to analyze computed wind speeds obtained from analog and digital cross beam correlations. This was accomplished by monitoring the space and time variations of skylight emission with two remote photodetectors and then correlating the two signals. Of the six experiments examined, three provided results agreeable to the wind speeds obtained from cup anemometers (Runs 1, 2, and 3). Of the remaining three, Run 6 showed a fairly good agreement, once adjustments for the higher frequencies were made. Runs 4 and 5 did not provide results comparable to anemometer speeds, either because the correlation of the common signal had an equal likelihood of being positive or negative, or the beam separation was too long, resulting in no common signal.

Based on the initial feasibility studies, the cross beam technique can measure atmospheric wind speeds some of the time. This means that the present setup could not be used for atmospheric wind measurements on an operational basis. Since the present study employed only the available skylight, the present concepts may be applied in future studies to other wavelengths where identifiable fluctuations are present.

BIBLIOGRAPHY

Bendat, J. S. and A. G. Piersol, 1966: Measurement and Analysis of Random Data. John Wiley and Sons, Inc., New York, N.Y., 390 pp.

Fisher, M. J. and F. R. Krause, 1965: Local Measurements in Turbulent Flows Through Cross Correlation of Optical Signals. NASA TM X-53295, 66-75. (On file, NASA George C. Marshall Space Flight Center, Marshall Space Flight Center, Alabama).

Fisher, M. J. and F. R. Krause, 1967: The Crossed Beam Correlation Technique. J. Fluid Mech., 28, 705-717.

Klugman, E. H., 1969: Feasibility Studies of Crossed Beam Wind Detection Systems. IITRI Report J6113-24 (Monthly Progress Report), IIT Research Institute, Chicago, Ill., 3 pp.

Krause, F. R., J. A. Jones , and M. T. Fisher, 1967: Digital Analysis of Random Processes by Piecewise Estimated Covariance Functions. NASA Technical Report, 36 pp. (On file, Fluid Mechanics Division, George C. Marshall Space Flight Center, Marshall Space Flight Center, Alabama).

Sandborn, V. A. and D. J. Pickelner, 1969: Measurements of Wind Speeds with an Optical Cross Beam System. Presented at the Annual International Geoscience Electronics Symposium, April 16-18, 1969. Washington, D.C. (On file, Engineering Research Center, Colorado State University, Fort Collins, Colorado).

Stephens, J. B. and V. A. Sandborn, 1968: Remote Wind Detection with the Cross Beam Method at Tower Heights. Presented at the Third National Conference on Aerospace Meteorology. May, 1968. New Orleans, La. (On file, Fluid Mechanics Division, George C. Marshall Space Flight Center, Marshall Space Flight Center, Alabama).

Szmauz, L., 1967: The PAR Models 100 and 101 Correlation Function Computers. Princeton Applied Research Corporation, Princeton, New Jersey (T-149-20K-9/67), 8 pp.

Wolff, M. M., 1966: A New Attack on Height Measurement of the Nightglow by Ground Triangulation. J. Geoph. Res., 71, 2743-2748.

APPENDIX

Distribution of Energy at Various Frequencies

By use of a 1/10 octave band width spectrum analyzer, the energy distribution at different frequencies can be obtained. Table 3 shows the original data as well as computations of the spectral density for each run. The quantity e^2 is the energy estimate at a given frequency and e_T^2 is the estimate of total energy. For comparison purposes, the spectral density is normalized by dividing $S(f)$ by e_T^2 .

Table 3. Original Data for Computing Spectral Density $\hat{S}(f)$ for Runs 1-6.

RUN 1	BEAM A				BEAM B			
f	e^2	$\frac{e^2}{f}$	$\frac{e^2}{e_T^2}$	$\frac{e^2}{e_T^2 f}$	e^2	$\frac{e^2}{f}$	$\frac{e^2}{e_T^2}$	$\frac{e^2}{e_T^2 f}$
.100	1.386	13.86	.226	2.26	1.598	15.98	.326	3.26
.125	1.665	13.30	.271	2.17	1.756	14.05	.358	2.87
.150	1.976	13.20	.322	2.15	1.627	10.85	.332	2.21
.175	2.000	11.43	.326	1.86	1.792	10.24	.366	2.09
.200	1.948	9.74	.318	1.59	1.623	8.12	.331	1.66
.250	2.064	8.26	.336	1.35	1.717	6.87	.303	1.21
.300	2.076	6.92	.338	1.13	1.124	3.75	.229	.76
.400	1.378	3.45	.225	.56	.817	2.04	.167	.42
.700	1.136	1.62	.185	.26	.717	1.02	.146	.21
1.000	.924	.92	.151	.15	.742	.74	.151	.15
2.000	.664	.33	.108	.05	.406	.20	.081	.04
4.000	.444	.11	.072	.02	.302	.08	.062	.02

$$\hat{S}(f) = \frac{e^2}{e_T^2 f}$$

From Beam A, $e_T^2 = 6.135$. From Beam B, $e_T^2 = 4.900$.

Table 3 (Continued). Original Data for Computing Spectral Density $\hat{S}(f)$ for Runs 1-6.

RUN 2	BEAM A				BEAM B			
f	e^2	$\frac{e^2}{f}$	$\frac{e^2}{e_T^2}$	$\frac{e^2}{e_T^2 f}$	e^2	$\frac{e^2}{f}$	$\frac{e^2}{e_T^2}$	$\frac{e^2}{e_T^2 f}$
.100	1.276	12.76	.360	3.60	1.476	14.76	.375	3.75
.125	1.414	11.35	.402	3.22	1.879	15.03	.447	3.82
.150	1.345	8.97	.380	2.53	1.910	12.73	.485	3.23
.175	1.503	8.59	.424	2.42	1.750	10.00	.444	2.54
.200	1.568	7.84	.443	2.21	1.759	8.80	.447	2.23
.250	.983	3.93	.277	1.11	1.303	5.21	.331	1.32
.300	.685	2.28	.193	.64	.833	2.78	.213	.71
.400	.435	1.09	.123	.31	.557	1.39	.141	.35
.700	.282	.40	.080	.11	.202	.29	.051	.07
1.000	.249	.25	.070	.07	.169	.17	.043	.04
2.000	.133	.07	.044	.02	.067	.03	.017	.01
4.000	.156	.04	.041	.01	.100	.03	.025	.01

$$\hat{S}(f) = \frac{e^2}{e_T^2 f}$$

From Beam A, $e_T^2 = 3.543$. From Beam B, $e_T^2 = 3.938$.

Table 3 (Continued). Original Data for Computing Spectral Density $\hat{S}(f)$ for Runs 1-6.

RUN 3		BEAM A				BEAM B		
f	e^2	$\frac{e^2}{f}$	$\frac{e^2}{e_T^2}$	$\frac{e^2}{e_T^2 f}$	e^2	$\frac{e^2}{f}$	$\frac{e^2}{e_T^2}$	$\frac{e^2}{e_T^2 f}$
.100	.604	6.04	.271	2.71	1.123	11.23	.432	4.32
.125	.676	5.41	.304	2.43	1.373	10.98	.528	4.22
.150	.692	4.61	.311	2.07	1.050	7.00	.403	2.69
.175	.719	4.11	.323	1.84	.925	5.29	.355	2.03
.200	.665	3.33	.229	1.49	1.000	5.00	.384	1.92
.250	.523	2.09	.235	.94	.665	2.66	.256	1.02
.300	.522	1.74	.235	.78	.453	1.51	.174	.58
.400	.505	1.26	.227	.57	.307	.77	.118	.30
.700	.405	.58	.182	.26	.153	.22	.059	.08
1.000	.450	.45	.202	.20	.193	.19	.074	.07
2.000	.327	.16	.147	.07	.062	.03	.024	.04
4.000	.298	.08	.134	.03	.109	.03	.042	.01

$$\hat{S}(f) = \frac{e^2}{e_T^2 f}$$ From Beam A, $e_T^2 = 2.225$. From Beam B, $e_T^2 = 2.603$.

Table 3 (Continued). Original Data for Computing Spectral Density $\hat{S}(f)$ for Runs 1-6.

RUN 4	BEAM A				BEAM B			
f	e^2	$\frac{e^2}{f}$	$\frac{e^2}{e_T^2}$	$\frac{e^2}{e_T^2 f}$	e^2	$\frac{e^2}{f}$	$\frac{e^2}{e_T^2}$	$\frac{e^2}{e_T^2 f}$
.100	3.524	35.24	.238	2.38	4.022	40.22	.174	1.74
.125	4.715	37.72	.319	2.55	5.410	42.08	.235	1.88
.150	5.250	35.00	.355	2.36	6.360	42.40	.276	1.84
.175	5.886	33.63	.398	2.27	6.710	38.34	.291	1.64
.200	6.410	32.05	.433	2.17	7.700	38.50	.334	1.67
.250	7.265	29.06	.491	1.96	9.125	36.50	.394	1.58
.300	6.769	22.56	.457	1.85	10.690	35.63	.464	1.55
.400	4.849	12.12	.328	.82	9.690	24.23	.420	1.05
.700	2.095	2.99	.142	.20	3.946	5.64	.171	.24
1.000	1.255	1.26	.085	.09	2.619	2.62	.114	.11
2.000	.672	.34	.045	.02	2.134	1.07	.093	.05
4.000	.665	.14	.021	.01	2.423	.61	.105	.03

$$\hat{S}(f) = \frac{e^2}{e_T^2 f}$$

From Beam A, $e_T^2 = 14.800$. From Beam B, $e_T^2 = 23.050$.

Table 3 (Continued). Original Data for Computing Spectral Density $\hat{S}(f)$ for Runs 1-6.

RUN 5	BEAM A				BEAM B			
f	e^2	$\frac{e^2}{f}$	$\frac{e^2}{e_T^2}$	$\frac{e^2}{e_T^2 f}$	e^2	$\frac{e^2}{f}$	$\frac{e^2}{e_T^2}$	$\frac{e^2}{e_T^2 f}$
.100	1.435	14.35	.183	1.83	1.385	13.85	.238	2.38
.125	1.885	15.08	.241	1.93	1.736	13.89	.295	2.38
.150	2.260	15.07	.279	1.93	1.920	12.80	.328	2.19
.175	2.459	14.05	.312	1.70	2.048	11.70	.349	2.00
.200	2.700	13.50	.345	1.72	2.260	11.30	.386	1.94
.250	2.651	10.60	.339	1.36	2.363	9.50	.405	1.62
.300	2.689	8.96	.343	1.14	2.000	6.67	.342	1.14
.400	2.525	6.31	.322	.81	1.728	4.32	.295	.74
.700	1.789	2.56	.227	.33	.998	1.43	.170	.24
1.000	1.395	1.40	.178	.18	.685	.69	.117	.12
2.000	.846	.42	.108	.05	.293	.15	.051	.03
4.000	.442	.11	.057	.01	.143	.04	.025	.01

$$\hat{S}(f) = \frac{e^2}{e_T^2 f}$$ From Beam A, $e_T^2 = 7.825$. From Beam B, $e_T^2 = 5.850$

Table 3 (Continued). Original Data for Computing Spectral Density $\hat{S}(f)$ for Runs 1-6.

RUN 6		BEAM A				BEAM B		
f	e^2	$\frac{e^2}{f}$	$\frac{e^2}{e_T^2}$	$\frac{e^2}{e_T^2 f}$	e^2	$\frac{e^2}{f}$	$\frac{e^2}{e_T^2}$	$\frac{e^2}{e^2{}_T f}$
.100	5.046	50.46	.143	1.43	5.922	59.22	.164	1.64
.125	6.479	51.83	.184	1.47	7.126	57.01	.197	1.57
.150	7.439	49.59	.211	1.41	8.215	54.77	.227	1.51
.175	8.225	47.00	.234	1.34	9.300	53.14	.257	1.47
.200	8.464	42.32	.240	1.20	9.679	48.40	.267	1.34
.250	9.370	37.48	.266	1.06	10.950	43.80	.304	1.16
.300	10.390	34.63	.295	.98	10.800	36.00	.298	.99
.400	10.490	26.23	.298	.75	10.530	26.33	.291	.73
.700	9.480	13.57	.288	.48	8.720	12.46	.241	.34
1.000	8.316	8.32	.236	.24	7.384	7.38	.204	.20
2.000	5.794	2.90	.165	.08	5.450	2.73	.151	.08
4.000	3.015	.75	.086	.02	3.750	.94	.069	.01

$$\hat{S}(f) = \frac{e^2}{e_T^2 f}$$

From Beam A, $e_T^2 = 35.200$. From Beam B, $e_T^2 = 36.200$.